RESEARCH ARTICLE

Seismic Hazard and Site Suitability Evaluation Based on Multicriteria Decision Analysis

**SAYED S. R. MOUSTAFA[1], MOHAMED S. ABDALZAHER[ID][1], (Senior Member, IEEE),
MUHAMMAD NAEEM[2], AND MOSTAFA M. FOUDA[ID][3], (Senior Member, IEEE)**

[1]Egyptian National Seismic Network (ENSN) Laboratory, Seismology Department, National Research Institute of Astronomy and Geophysics (NRIAG), Helwan, Cairo 11421, Egypt
[2]Exploration Department, Mari Petroleum Company Ltd., Islamabad 44000, Pakistan
[3]Department of Electrical and Computer Engineering, Idaho State University, Pocatello, ID 83209, USA

Corresponding author: Mohamed S. Abdalzaher (msabdalzaher@nriag.sci.eg)

ABSTRACT Effective management and planning for sustainable urban regions' development require up-to-date information. Natural hazard maps (NHMs) creation is critical for urban development. Urban areas along the western coast of Saudi Arabia are susceptible to natural disasters due to their hazard sources' proximity, especially, with the lack of preparation. Yanbu' Al-Bahr, a major Red Sea port, provides an excellent example. This research aims to combine NHMs into a single multi-hazard map, allowing acceptable site identification for urban development. To create a seismic hazard model of the rapidly growing Yanbu' Al-Bahr region, spatial distributions of different hazard entities were assessed using the analytical hierarchy process (AHP). To create a multi-hazard map, six seismic hazard assessment maps were independently developed. Hazard attributes were assimilated into a geographic information system (GIS) platform to delineate seismic hazard zones and build a suitability map for urban development. Weight and rank values were determined during AHP and assigned to each layer and its corresponding classes. By overlaying all the weighted maps, a suitability map was created. This map depicts the research area's prospective appropriateness for urban growth. Accordingly, the study area was classified into five hazard categories, namely, very-low (VL), low (L), moderate (M), high (H), and very high (VH). Therefore, the limited regions, most appropriate locations, and least suitable areas were identified. Accordingly, stakeholders can use the produced seismic hazard map as a platform for future land-use planning and environmental hazard management. Furthermore, the AHP-GIS model would deliver more precise findings in urban development site selection studies.

INDEX TERMS Seismic hazard, multi-criteria analysis, AHP, GIS, urban planning, Yanbu' Al-Bahr, Saudi Arabia.

I. INTRODUCTION

Urban areas can be significantly influenced by several side effects such as dense industrial activity, rapid planned construction, fragmentation of natural habitats, and degradation of surface and ground waters by a wide range of chemical contaminants [1]. The hazardous nature and effects of earthquakes need to be carefully considered when designing structures and facilities [2]. Besides, both planning, growth, and management of urban environments are typically

The associate editor coordinating the review of this manuscript and approving it for publication was Le Hoang Son[ID].

determined by economic and social considerations, at the expense of the potential geological and environmental threats [3]–[5]. Meanwhile, these omitted threats can cause extensive damage to the social and economic environments, and loss of human life and property in areas vulnerable to natural hazards [6], [7].

To reduce the aforementioned effects, certain physical and/or geological parameters of surface or subsurface rocks in urban areas and their vulnerability to earthquake hazards should be effectively considered beforehand [8], [9]. As a result, a procedure for shortlisting sites is needed to pick the most ideal places for applying site-specific micro zonation

methods [10]–[12] nature-based seismic hazard reduction measures. To guarantee sustainable land management and the protection of human life in urban environments, decision-makers, engineers, planners, and managers must consider the physical elements of the urban region, as well as natural risks, while planning and growing an urban environment [13], [14].

A seismic hazard index model can effectively minimize the adverse effects of nature-induced hazards [15]. The datasets required for the development of such a model should be geographically related to each other. Moreover, an appropriate decision-making support tool is needed to incorporate all hazardous components, as per their expected contribution to overall risk [15]–[19]. In this regard, Multi-criteria decision analysis (MCDA) is among the tools that can be used to process complex decision constellations for technological, ecological, economic, and social aspects [20]. MCDA techniques are decision-making tools for dealing with complex choice circumstances that need taking into account technological, economic, environmental, and social variables. These technologies have been combined with geographic information systems (GIS) on several occasions, making them excellent for improving land-use planning [3], [13], [21]–[23].

To reasonably plan and use the MCDA, the various criteria contributing to the decision-making process have to be ranked and weighted, as per their relevance and importance [20]. Analytic Hierarchy Process (AHP) [24], [25] has recently become attractive as a sufficient MCDA tool with potential for various uses [15], [26]–[35]. Interestingly, combining the AHP with a GIS platform leads to optimizing a site-specific seismic design and planning [36], [37], as well as enhancing the scope of conventional hazard assessment maps [8]. This provides vital information for structural engineering applications, urban planning, hazard mitigation, and management [20], [38], [39]. Optimization also contributes to accurate data observation and management [40]–[49]. AHP is also considered one of the most promising techniques for assessing weightings [36], [37] of the various utilized entities. As a well-established mathematical evaluation method [24], AHP assists in decision-making by assigning ranks and weights to the employed attributes through a matrix operation. In addition, it utilizes the hierarchical structures to quantify relative priorities for a specified set of elements on a ratio scale [24].

In this study, the area of interest is Yanbu' Al-Bahr. It is located within Al-Madinah province and is considered one of the main seaports of Saudi Arabia (Figure 1). Furthermore, it significantly contributes to industrial and commercial activities [22]. The area was planned to serve as a leading zone for providing a strategic outlet to the Red Sea shipping lanes on the western coast of Saudi Arabia [50]. The motivation for presenting an integrated seismic hazard of the Yanbu' Al-Bahr area is its vulnerability to expected natural hazards from active tectonics. Accordingly, we prepared a seismic hazard index map for the area using the AHP technique and taking into account several earthquake-triggering parameters, namely, site amplification (SA), fundamental frequency (FF), overburden sediment thickness (ST), overburden sediment

strength (SS), seismic vulnerability index (k_g), and peak ground acceleration (PGA) [12]. Previous studies have considered either seismological parameters or geological parameters individually, and not in an integrated manner [22], [51]. Unlike the previous traditional studies, to the best of our knowledge, this is the first to integrate several seismic layers on a GIS platform to derive a reliable seismic hazard model map for the present study area.

This paper's major basic contributions can be summarized as follows:

- We propose a novel crucial criterion for reducing the negative environmental, physical, and economic impacts of urban and industrial facilities.
- We consider the site suitability for urban development, especially near marine active seismic sources like the Red Sea where the suitability analysis of site selection is implemented using the GIS platform to determine the best place or site for urban development. To the best of our knowledge, no similar study has been presented for the same area.
- We integrate the GIS and AHP for developing a fast seismic hazard assessment.
- We determine the most accurate criterion weights, which are examined by various investigations.
- We create an appropriate map of urban and industrial sites for the Yanbu' Al-Bahr region. To the best of our knowledge, no similar map has been created before for the same area.

The rest of the paper is organized as: Section II portrays the motivation of the study. Afterward, Section III presents the geological and seismological settings and data analysis. Section IV indicates the preparation of attributes maps. The developed seismic hazard, suitability assessments maps, and results are then introduced in Section V. Finally, the paper is concluded in Section VI.

II. MOTIVATION
The present study focused on developing a seismic hazard map for the Yanbu' Al-Bahr area (Figure 1), to provide a platform for further investigation and urban development. Geologically (Figure 3), the study area is a part of the Arabian Shield and is mostly covered by outcrops of Upper Proterozoic rocks. Locally, Cenozoic basalt flows and Aeolian sand deposits overlie these older rocks. A narrow coastal strip in the area is made up of Tertiary-Quaternary marine and continental coastal plain sediments [52]. According to the observed geological setting, erosion and subsequent deposition of the Tertiary sediments are controlled by faulting [53] and graben formation attributed to the Najd fault system [52], [54].

It is well known that similar studies to ours have been performed in other places in the world [10]–[12]. However, such type of studies is very few for Saudi Arabia in general and Yanbu' in particular. Moreover, to the best of our knowledge, no similar study has considered the site suitability for urban development, especially near marine active seismic sources
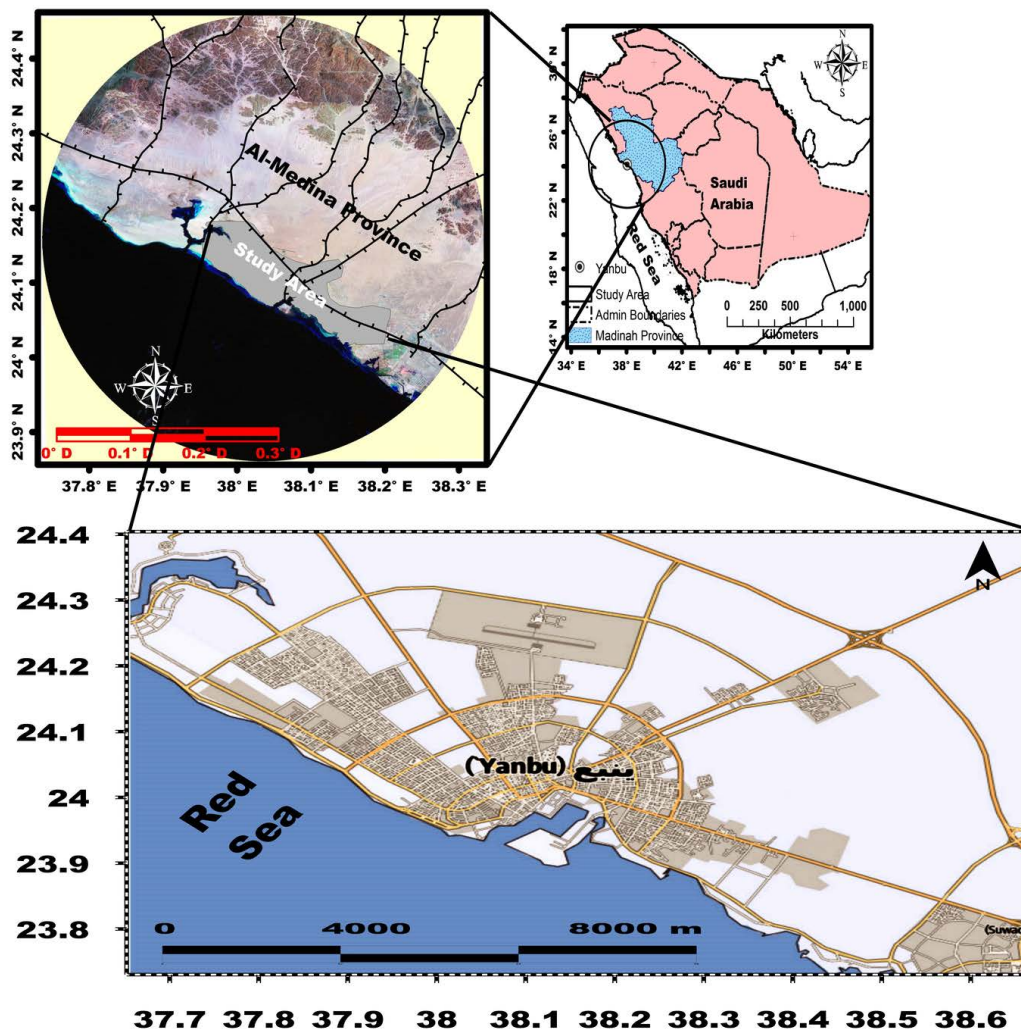
FIGURE 1. Location map of Yanbu' Al-Bahr area.

like the Red Sea. This study outlines a novel site selection approach that may be used to rate potential sites based on the appropriateness of seismicity to decrease natural hazards on a site-specific level. This article focused on the use of the AHP and GIS to discover the best locations for urban developments. As a result of this investigation, a total of 6 major criteria and 33 sub-criteria were employed for this study by suggesting additional significant and crucial criteria to the criteria currently found in the literature. AHP was used to weight the criterion, and GIS was used to analyze all data pertaining to these criteria for the Yanbu' Al-Bahr area. At the conclusion of the study, a suitability map for urban and industrial sites and limited zones in the study area was created. Accordingly, the above-mentioned essential reasons are the main incentive to study this area.

III. GEOLOGICAL AND SEISMOLOGICAL SETTINGS AND DATA ANALYSIS

The mapped area is located on the western Red Sea coast of Saudi Arabia, about 350 km north of Jeddah city

(Figure 1). This region has been developed on what used to be a desert plain, occupied only by a few agricultural dwellers. This is rapidly expanding as an industrial and commercial center [55], [56]. The surface geology of the area is dominated by Tertiary and Quaternary sedimentary deposits (Figure 3), outcropping along a narrow Red Sea coastal plain with an average width of 5–10 km [52], [57]. It is worth mentioning that the root-mean-square (RMS) values for most of the georeferenced maps were less than half the pixel size of the map (30 m).

Because of its proximity to the active Red Sea tectonic zone, the area is subject to geodynamic processes operating in the region [58]–[60]. Historical earthquake information [61], [62] and recent seismotectonic studies [54], [58], [59] reveal significant earthquake activity in the Yanbu' and surrounding areas, mostly emanating from the Red Sea rift zone. In 1068 AD, the region suffered significantly because of an earthquake with its origin in a nearby region [58], [59]; based on the Modified Mercalli Intensity (MMI) scale, the intensity of that earthquake has been estimated to be level VI [54],
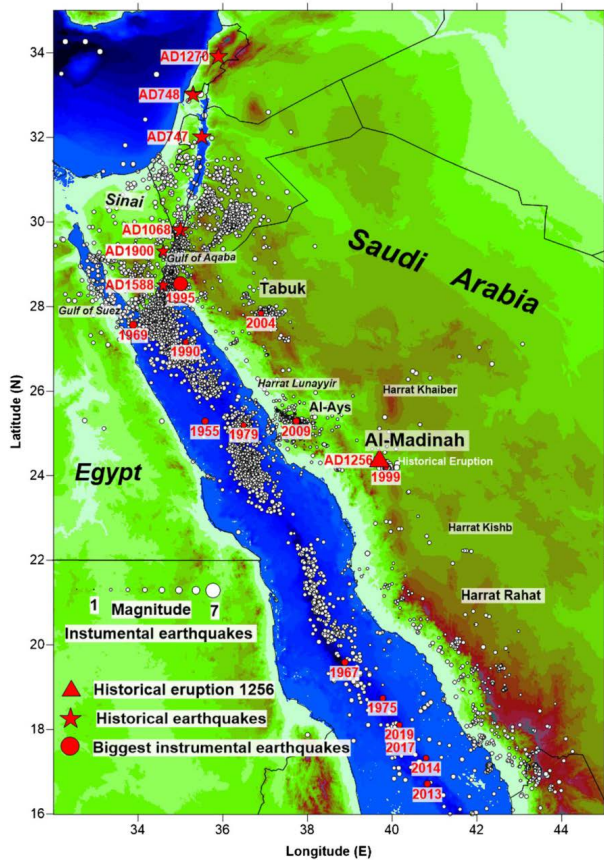
FIGURE 2. Spatial distribution of the main events affecting Yanbu' [66].

[58], [59], [61]. The spatial distribution of instrumental earthquakes (Figure 3b) indicates that seismic activity in the area is not only related to the rift zone [22], [54], [58], [59], [61], [63], but also to neighboring tectonic zones in the Arabian Shield [54], [58], [61], [63]. Earthquakes in Tabuk (2004) and Badr (2009) are examples of seismic events that have affected regions at some distance from the rift zone. On 19 May 2009, the area was struck by a swarm of M-sized earthquakes (from a source in the volcanic field or Harrat Lunayyir) with a moment magnitude (M_w) of 5.7 [15], [22], [59]. The epicenter of this activity was located about 120 km southwest of Yanbu' city. The earthquake was followed by a number of aftershocks with a maximum magnitude of 4.2 [64], [65] and ground-shaking intensity of level V on the MMI scale [15], [22], [59], [65]. Spatial distribution of the main events affecting the mapped area is shown in Figure 2 [66].

A. DATA GATHERING AND ANALYSIS
To assess seismic hazards in the Yanbu' Al-Bahr area, the most relevant parameters affecting the suitability of nature-based strategies for seismic hazard reduction were identified through a careful literature review. The drawbacks of such strategies were also noted. Various geological, seismological, and geophysical features were taken into consideration. This assessment is mainly geared toward the identification and characterization of major parameters used in the

final integrated seismic hazard map and characterization of major influential parameters to be used in the final integrated site-suitability maps.

1) GEOLOGICAL FEATURES
Collected geological raster images were scanned and georeferenced, so that these could be overlain with other collected vector data (Figure 3(a)). Additionally, faults were digitized using the georeferenced geological maps of Yanbu' Al-Bahr [52], [69] and Al-Madinah Quadrangles [57], as depicted in Figure 3(a).

Collected surface geological data of the mapped area indicates that it is mainly composed of Tertiary and Quaternary deposits. These are situated along the narrow coastal plain of the Red Sea, with average areal coverage from 5 km to 10 km [52], [57], [69] and a total of 2-5 m thickness. The observed scattering of Tertiary deposits is thought to be controlled by syndepositional graben faulting connected to Red Sea rift evolution [52], [69]. Sands and gravels are the main Quaternary deposits found along the coastal plain of the mapped area. Sandy sediments cover wide areas and have a composite origin integrating rocks transported by both fluvial and Aeolian sources. Observed gravel rocks are thought to be related to the degradation of older terraces [52], [69]. A very close drainage network dissects sediments in the mapped area, which are closely linked with recent alluvium deposits.

2) SEISMOLOGICAL FEATURES
For the proper development of a seismic hazard model for the Yanbu' Al-Bahr area, a homogeneous earthquake catalog needed to be prepared. For this purpose, datasets from reputable international sources, including the United States Geological Survey (USGS), the International Seismological Center [67], and the Global Centroid-Moment Tensors [68], [70], [71] were collected. Local earthquake databases from Saudi research institutions (i.e. King Saud University (KSU), King Abdul Aziz City for Science and Technology (KACST), and SGS) were also used. The complete catalog period (1964–2020) contains a total of 10,231 events; of these, 739 were of magnitude $2.0 \leq M_w \leq 4.0$ and 22 events were of magnitude $4.0 \leq M_w \leq 5.7$. Figure 3(b) depicts the spatial distribution of all collected events from the various utilized data sources, along with the geological faults affecting the mapped region.

Homogenization of the collected earthquake catalog is also a prerequisite for proper seismic hazard assessment. This requires region-based magnitude conversion relationships for the various earthquake magnitudes collected. The general orthogonal regression (GOR) and random sample consensus (RANSAC) regression techniques [43], [72]–[75] were utilized for preparation of the homogenized M_w catalog.

A circular seismotectonic map (Figures 1 and 3(b)) with a radius of approximately 280 km around Yanbu' city was prepared from observed faults/lineaments and associated seismicity of the study area. This map shows both normal and transformed faults running parallel and/or across the Red Sea.

(a) Surface Geology

(b) Faults, Seismicity and Seismogenic zones.
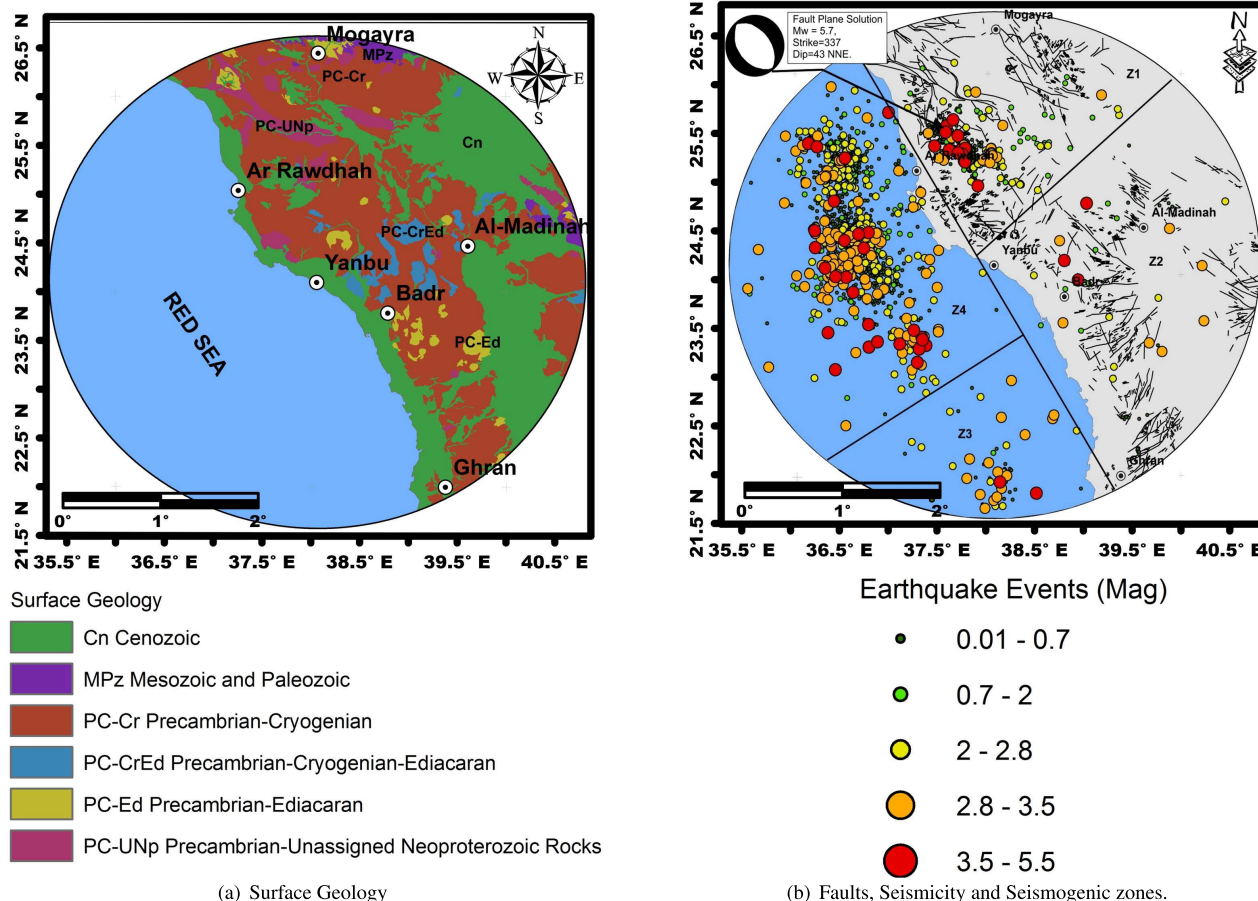
FIGURE 3. (a) Surface geological setting of the area (modified after [57]). (b) Regional seismotectonic map of the study region and surroundings, depicting major linear tectonic features with seismicity covering 1964–2020. Earthquake epicenter data were collected from the International Seismological Center [67] and the Saudi Geological Survey (SGS). Faults were digitized from the geological map of the Al-Madinah quadrangles [57]. Z_1, Z_2, Z_3, and Z_4 are the four seismogenic zones utilized in our analysis. Beach-ball represents the focal mechanism of the Al-Ays earthquake, adopted from the Global Centroid-Moment Tensors (GCMT) database [68].

Some of these faults extend inland for tens of kilometers [76], [77]. Due to relative movements along these faults, one can expect large and damaging earthquakes in the region [78].

Based on the spatial distribution of seismic events (and corresponding fault plane solutions), the region was divided into four seismotectonic source zones. Seismic source zones lying within a 280 km radius are considered potentially hazardous for the area, while those outside the radius are unlikely to significantly influence expected ground motion (Figure 3(b)).

The first zone (Z_1) is located northeast of the study region, about 100 km from Yanbu' city. It is characterized by dense clustering of earthquakes, with the maximum-recorded magnitude being from the 2009 Al-Ays event. Major tectonic features in this zone are aligned in an NW-SE direction, almost parallel to the Red Sea trend [64], [79]. Maximum faults in this zone follow an NW trend and are interpreted to form a part of the Najd Fault System [80].

The second zone (Z_2) is characterized by a few scattered seismic events without any clear trend, with the maximum

reported magnitude being that of the 2009 Badr event. Both Z_1 and Z_2 are linked to intra-plate seismic sources influenced by Red Sea tectonics [64], [79].

The third seismic source zone (Z_3) is located about 200 km southwest of Yanbu' city, with a maximum magnitude of 3.9 and NE-SW-directed tectonic features. The fourth source zone (Z_4) is another dense-clustering NW-SE directed zone that attains events with a maximum magnitude of 4.6. Seismic activity in both Z_3 and Z_4 is mainly related to the Red Sea rifting [58], [61], [63].

To analyze the significance of influencing earthquakes and to identify areas where ongoing deformation could lead to future earthquake hazards, the density of earthquakes occurring over the last fifty years was assessed. The strong density of seismic activity was noted in zones Z_1 and Z_4, as indicated by the large red-colored circles in Figure 3(b). In terms of earthquake density/intensity, five zones (very low (VL), low (L), moderate (M), high (H), and very high (VH)) were identified, with areas vulnerable to natural hazards (H earthquake density) clearly distinguished [22], [54], [58], [59], [61], [63].

3) SURFACE GEOPHYSICAL FEATURES

The local surface geology and soil properties of the Yanbu' Al-Bahr region significantly influence the expected intensity of potential earthquake ground motion. The local site response of an area, therefore, plays an important role in seismic hazard mapping. In the current research, the single-station microtremors survey method was utilized to determine the dynamic characteristics (FF and SA factor) of Yanbu' Al-Bahr sediments by applying the horizontal-to-vertical spectral ratio (HVSR) technique [81]. The reliability of this method has been tested both numerically [82] and experimentally [83].

Microtremors were measured at twenty-three sites using a portable Tromino 3G seismograph [84] with three orthogonal electrodynamic velocity sensors with a frequency range of 0.2–10 Hz, a GPS receiver, a digitizer, and a recording unit. All parts of this system were integrated with a single box unit to minimize expected electronic and mechanical noises. Site Effects Assessment Using Ambient Excitations (SESAME) guidelines [85], [86] were followed for analysis of microtremor data by first selecting a stationary portion of the whole record using at least 20 windows of 25–60 s length.

Following this, each window of the record was detrended and tapered (5% cosine), fast Fourier transformed (FFT), and then smoothed. No significant differences were noted in obtained results after testing several smoothing procedures. The time-dependent spectra of the collected data (ratiograms) are utilized to discriminate between the presence of real dominant frequencies linked to resonances of the subsurface structure and the spurious appearance of peaks due to local transients. No filtering was applied before FFT, and a check was made to guarantee the absence of anthropogenic disturbances, i.e., monochromatic sources [81], [83].

Two horizontal component spectra were combined into RMS before division by a vertical component spectrum. Finally, the geometric means and standard deviations of the HVSRs were calculated for frequencies >0.4 Hz, with this threshold chosen to avoid the Eigen frequency of the sensor (0.2 Hz). Moreover, and to upsurge the spatial and azimuthal coverage of microtremor observation points, results from the previous microtremor HVSR surveys of [87] and [88] were integrated after performing a comparative analysis of our data with their datasets. This analysis revealed compatibility between our respective datasets within a 10% error range.

As shown in Figure 4, the fundamental frequency (FF), and matching peak amplitude or site amplification (SA) at the measured sites were determined over the targeted area.

Finally, to develop a reliable seismic hazard model for the study area, the spatial distribution of selected events for this study and all available geological and geophysical information (surface and subsurface) were incorporated into a spatial geodatabase. This was created using ArcGIS [89], [90] modules.

B. ANALYTIC HIERARCHY PROCESS (AHP)

After the important elements have been identified, the AHP will be used to determine the relative relevance of each one in determining site suitability for the implementation of nature-based approaches. The AHP method is among the oldest and most used multi criterion-decision analysis approaches. Moreover, it has remarkable benefits such as usability, effortlessly reasonable system, separating the problem into simple pieces, and working independently on authentic information sets. When contemplating the use of nature-based solutions to decrease seismic danger at sites, all of the factors outlined would not be of equal value [24].

To establish the relative importance of each factor, the AHP was used. With limited data, the AHP proved to be beneficial for evaluating situations requiring various and diverse criteria [91]. In a multi-criteria evaluation problem, the AHP demonstrates flexibility in dealing with both qualitative (intangible) and quantitative (tangible) elements. In addition, the AHP provides a scientific framework for detecting and correcting inconsistencies in interpreting the relative importance of components in a site appropriateness analysis [27].

A seismic hazard model for the Yanbu' Al-Bahr area was prepared using the AHP technique [24]; this is considered to be one of the most commonly applied procedures for M_cDA problems. The AHP method is utilized to analyze the structure of the seismic hazard selection problem and to estimate the appropriate weights of implemented criteria for final ranking. In this procedure, criteria that have the greatest effect on the creation of the seismic hazard model are determined via sensitivity analysis.

The AHP encompasses the decomposition of the complex seismic hazard problem into a multilevel hierarchical structure of objectives, criteria, and alternatives. This is based on previous relevant studies, fieldwork observations, and experiences. In the case of Yanbu' Al-Bahr and after an intensive literature review, selected literature [22], [50]–[52], [54], [56], [87], [88] was found to be very useful for breaking down the complex seismic hazard problem.

Once the hierarchy was established, we proceeded to assess the relative importance of considered decision criteria, then compare the decision alternatives concerning each criterion, and finally decide on the inclusive priority and corresponding ranking of each decision alternative. Determination of the relative importance of implemented decision criteria and the comparison of decision alternatives concerning each criterion were carried out through pairwise comparison. This involves developing a comparison matrix at each level of the hierarchy, calculating the relative weights of each element of the hierarchy, and estimating the Consistency Ratio (CR) to check the consistency of judgment. Indeed, calculating the comparison

matrix is adopted from [24], [92], [93], which is derived by:

$$A = \begin{bmatrix} w_1/w_1 & w_1/w_2 & \cdots & w_1/w_n \\ w_2/w_1 & w_2/w_2 & \cdots & w_2/w_n \\ \vdots & \vdots & \ddots & \vdots \\ w_n/w_1 & w_n/w_2 & \cdots & w_n/w_n \end{bmatrix} \quad (1)$$

where w is the weight of n set objects. Accordingly, A is the ratio of one weight over another. The consistency of the pairwise matrix (CI) is defined as [24]:

$$CI = \frac{\lambda_{max} - n}{n - 1} \quad (2)$$

where n is the order of the matrix and λ_{max} is the largest or principal eigenvalue of the pairwise comparison matrix and is used as a reference index to screen information by calculating the CR of the estimated vector. CR can be given by [24]:

$$CR = \frac{CI}{RI} \quad (3)$$

where RI is the random consistency index obtained from a randomly generated pairwise comparison matrix. More particularly, RI of size n is the average CI calculated from a large number of randomly generated reciprocal matrices by computer [94]. For acceptable comparisons, the value of the CR must be < 0.1. If CR ≥ 0.1, the values of the ratio are considered indicative of inconsistent judgments [24]. After all the pairwise comparison matrices were established, the vector of priority weights was computed based on Satty's eigenvector, after normalizing the pairwise comparison matrix over the entire hierarchy.

IV. PREPARATION OF ATTRIBUTES MAPS

The proper deployment of nature-based approaches necessitates a thorough examination of site-specific factors. Factors including site effects, sedimentary cover strength and thickness, seismic ground vulnerability, and peak acceleration should all be evaluated.

The seismic hazard map for the Yanbu' Al-Bahr area was prepared through analysis and spatial integration of several earthquake triggering attributes on the GIS platform. Six factors were chosen in this study to determine the most appropriate areas for applying nature-based methodologies, and they are outlined and summarized below.

The seismic hazard map for the Yanbu' Al-Bahr area was prepared through analysis and spatial integration of several earthquake triggering attributes on the GIS platform.

A. SITE AMPLIFICATION (SA) AND FUNDAMENTAL FREQUENCY (FF)

The method utilized for estimating SA and FF values (shown in Figure 4) was the HVSR of [81]. The first step was to perform a Fourier transformation of three-component microtremor records. The ratio of the Fourier amplitude spectra between horizontal and vertical components was then calculated.

The estimated SA and FF parameters were then gridded using the Kriging method [95], [96] and contoured, as can be seen in Figure 4. It is worth mentioning that Kriging outperforms the corresponding GIS techniques in many points such as measuring uncertainty attached to the results and performing spatial anisotropy, and the independency of the observations range used for interpolation.

The superposition of different soft layers may cause amplification at a site due to modifications of incoming earthquake waveform characteristics. Based on the estimated values, the region as a whole is characterized by lower SA values, except in a small area in the north (Figure 4(a)). SA effects are therefore dependent on the type of sedimentary layer and its thickness [97], [98]. Higher SA values (>3.97) can generally be observed along the coastal area with a relatively thick sedimentary cover.

On the other hand, and as indicated in Figure 4(b), the Yanbu' region exhibits varied FF values (from a minimum of 1.4 Hz to a maximum of 7.21 Hz). The majority of the mapped area reveals L FF values (1.4–2.57 Hz).

The spatial distribution of the FF layer indicates the maximum concentration of the FF values in central areas with a gradual decrease towards the northern part and in the Red Sea direction, which indicates probable thick sedimentary cover. The zones with H FF could be either due to hard-consolidated soil or compact subsurface structures. SA in the study area has been mainly attributed to different patterns of radiation from sources, scattering, diffraction, and undulating topographic effects [87], [88]. The layers related to amplification and frequency attributes reveal that solid/stable rocks dominantly cover the study area. However, the western part, which lies along the Red Sea coast, is more stable as compared to that located away from the shoreline in the east.

B. SEDIMENT STRENGTH (SS) AND SEDIMENT THICKNESS (ST)

The time-averaged shear-wave velocity in the upper 30 m (V_S^{30}) is a dynamic property that can be used to estimate in-situ granular sediment strength (SS) and is commonly used for site classification [99].

It is worth mentioning that site characterization, in terms of soil strength, is a critical attribute of seismic hazard assessment because local geology has a substantial effect on earthquake ground motion [97], [98].

For the development of the SS map in terms of V_S^{30} values, two approaches were used. In the first approach, the experimental HVSR curve was fitted with a synthetic curve using the independently-known thickness of a superficial subsoil layer from boreholes [78] as a constraint [100]. The underground shear-wave velocity structure was obtained through modeling of the HVSR curve by using the Phase Velocity Spectra Module in Grilla software [101], which assumes a vertically heterogeneous, one-dimensional elastic model. This assumption was verified by taking several HVSR recordings and comparing them. All selected cases showed essentially identical HVSR curves and thus the assumption of
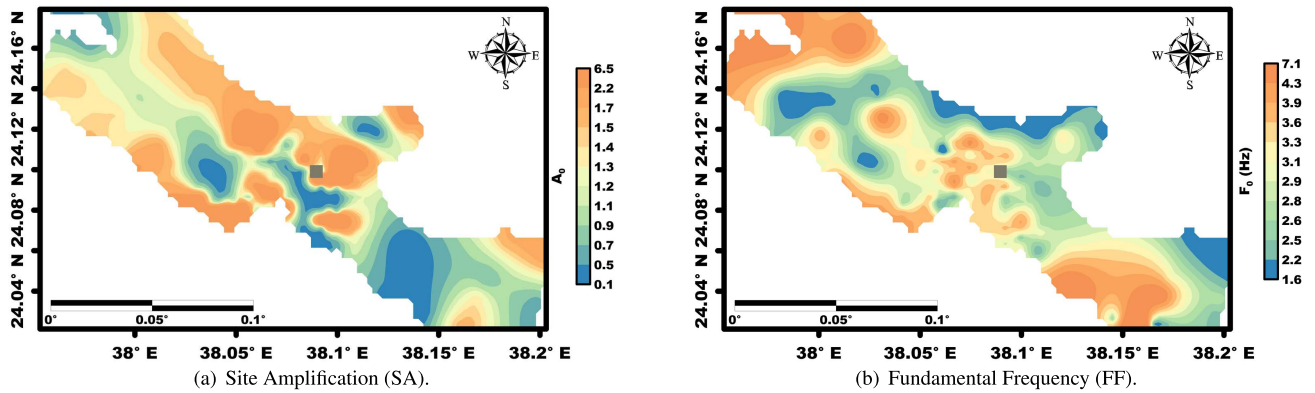
FIGURE 4. Spatial distributions of site amplification (SA) (a) and fundamental frequency (FF) (b) thematic layers over the mapped area.

1-D appeared to be very well satisfied. The fitting procedure included depth determination of the shallow stratigraphic horizons from boreholes [78], [88]. These values were then used as a constraint to fit the experimental HVSR curve with the theoretical one (Figure 5(a)). A trial-and-error procedure was used to obtain a shear-wave velocity versus depth profile (Figure 5(b)). Once a satisfactory fit with the HVSR curve was obtained, the geometry of the layers and layer velocities were fixed to estimate the final value of V_S^{30}. A synthetic curve was drawn by assuming a stratified one-dimensional soil model and a microtremor wavefield [100] from distant random Rayleigh wave sources (Figure 5(a)).

In other locations for which borehole information was not available, the procedure introduced by [102] was utilized to develop a new FF-based proxy measure for V_S^{30}. The developed model (depicted in Figure 5(c)) is only applicable when FF >2.5 Hz. The mean absolute difference between V_S^{30} values from boreholes and those estimated by the aforementioned empirical relation is ≈7%. In the end, V_S^{30} data were used for the preparation of the shear-wave velocity distribution map of the study area in the topmost 30 m of sediments. Consequently, and based on our estimation, V_S^{30} values for the study area stand between 180 m/s and 240 m/s (Figure 5(d)).

The overburden ST is an important geological parameter that significantly contributes to spatial variations in ground motion during an earthquake. Several studies [103]–[105] have shown that microtremor measurements can be used to map ST. According to [103], the FF of any sedimentary layer is closely related to its thickness (ST) through the relation:

$$ST = a \times FF^b \qquad (4)$$

where a and b are empirically-determined constant parameters. More particularly, a and b are determined from regression analysis between overburden ST and FF. Besides, the developed equation is illustrated by Figure 6(a).

Available borehole data with known thickness are used as constraints for theoretical modeling of the HVSR curve (Figure 6(a)). Without a constraint, infinite models can fit

the same HVSR curve. Thus, by assuming a stratified, one-dimensional soil model for the wave field and for the medium, a theoretical HVSR curve was fitted to the experimental one to infer a subsoil model [97], [98], [105]. This allowed classification of the sedimentary cover, which was used for seismic hazard assessment. It can also guide the choice of the optimal response spectrum in any future study, at least when ST > 30 m. The distribution of the V_S^{30} parameter categorized soils in the study area into C and D types, as per the classification of the Building Seismic Safety Council [99], as shown in Figure 6(b).

The HVSR of microtremors was calculated for sites close to boreholes, where the thickness of the sedimentary cover was known. The empirical relation between ST and FF of the main peak in the H/V spectral ratios was calculated (Figure 6(a)). The new relationship, validated for the area of Yanbu' Al-Bahr, yields better estimates of the thickness of the ST cover (Figure 6(b)). Across the study area, loose fine to medium sand deposits was observed located between the surface and a depth of 15 m below, with a very shallow groundwater table (<1m). A thin surficial layer (2–5 m) of compact shattered coral reef was also observed. This layer is underlain by a thick layer of very loose to loosen fine sand with some recorded gravel and/or silt deposits (6–8 m) below ground level. Some areas also show a dense to a very dense layer of silty sand with gravel and cobbles. South of Yanbu' city, coral limestone is interbedded with fine coralline sand, which is dense to very dense in deeper parts of the layer [78]. It was observed that the central part of the study area is characterized by a thick section of soft sediments, which can amplify ground-shaking intensity four to five times more than that of the underlying bedrock. Using all of the noise measurements carried out in the area, the new equation allows us to calculate ST over a wider area. Our results confirm the suitability of the H/V ratios of seismic noise as a geophysical exploration tool, at least in geological structures with significant impedance contrast between sedimentary layers and bedrock.

In the present study, microtremor measurements were made at several sites where ST is known from boreholes and seismic refraction studies [78]. These data were then used in

(a) HVSR fitting.

(b) V_S^{30} model.

(c) Developed relation.

(d) V_S^{30} distribution.
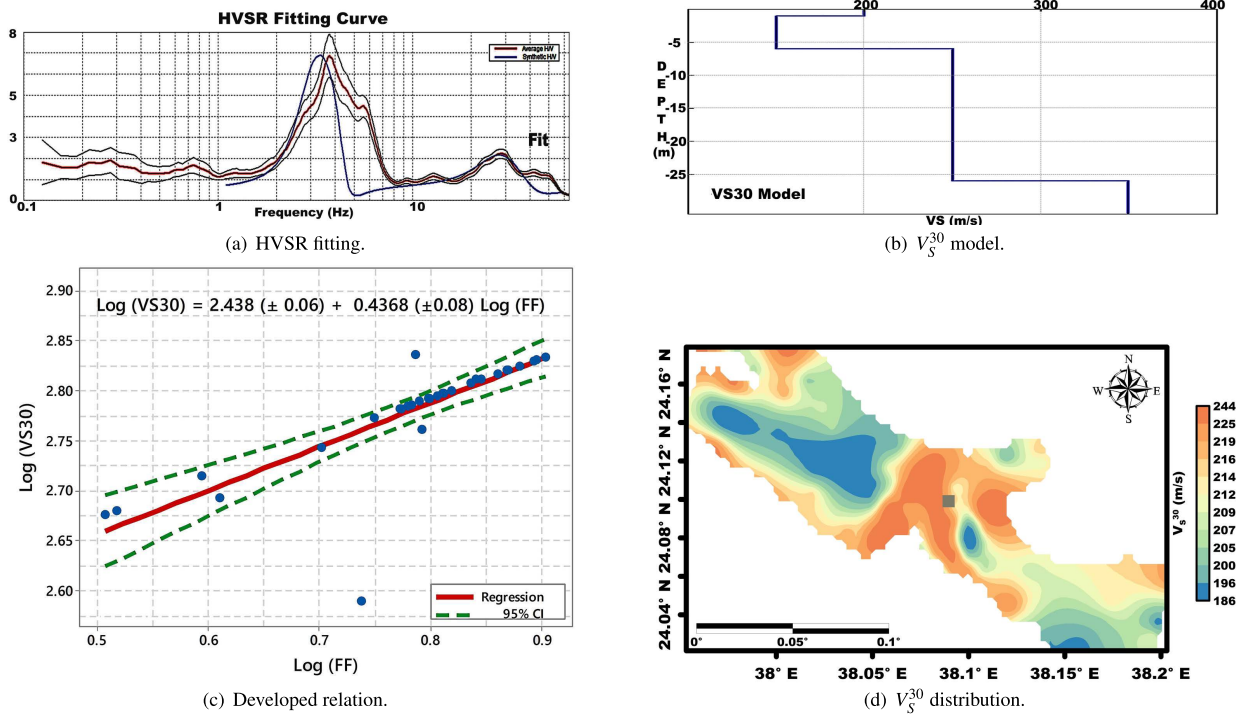
FIGURE 5. (a) Correlation between theoretical modeling of the HVSR curve (blue line) transfer function with the average HVSR curve (red line) to estimate V_S^{30} model shown in panel (b). (c) Fitting of V_S^{30} values calculated from borehole data vs. fundamental frequency from HVSR spectral ratio (d) Spatial distribution of the effective soil strength in terms of shear-wave velocity in the upper 30 m (V_S^{30}).

(a) Developed relation.

(b) ST distribution map.
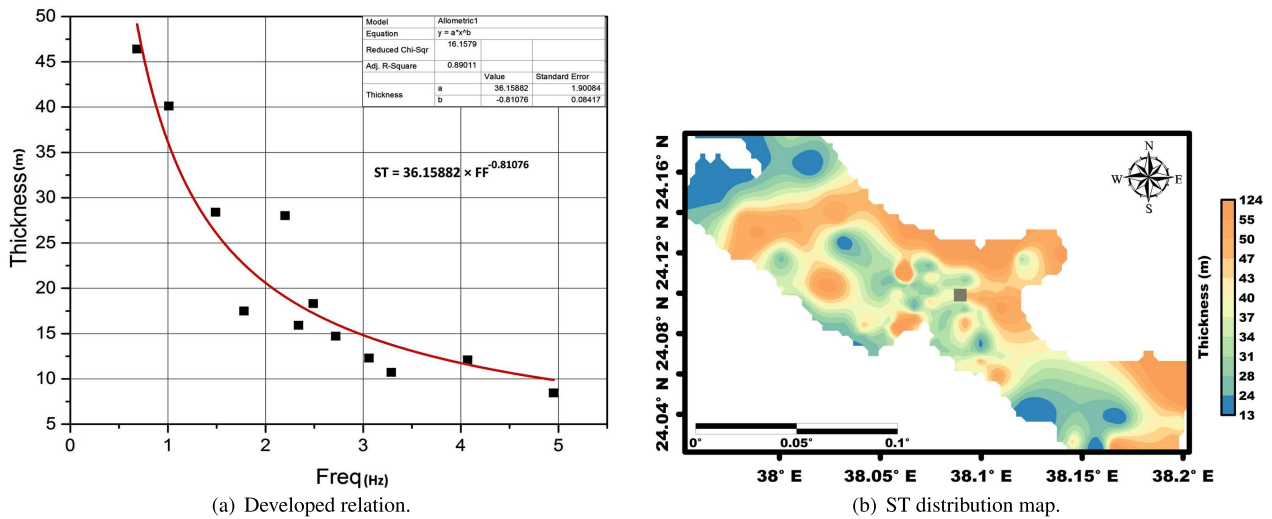
FIGURE 6. (a) Fitting of the fundamental resonant frequencies calculated from HV spectral ratio vs. ST from borehole data (a), the solid line represents a fit to data points and overburden ST (b) ST thematic layer distribution in the mapped area.

non-linear regression analysis using OriginLab [108], [109] to estimate the relation constants and ST.

A new empirical equation was developed for the Yanbu' Al-Bahr region, with an acceptable coefficient of determination ($R^2 = 0.89$), as shown in Figure 6(a). The mean absolute difference between ST values from boreholes and those estimated using the HVSR method was ≈9%. The overburden thickness in the study was consequently found to vary between 2–15 m but is predominantly in a range

of 3–6 m (Figure 6(b)). This shows that the most vulnerable areas to seismic hazards are those associated with thick to very thick sedimentary cover.

C. SEISMIC VULNERABILITY INDEX (k_G) AND PEAK GROUND ACCELERATION (PGA)

When seismic waves pass through sediments, pore pressure increases, the structure of sediments is distorted, and loosely-packed soils collapse. In this process, sediments can
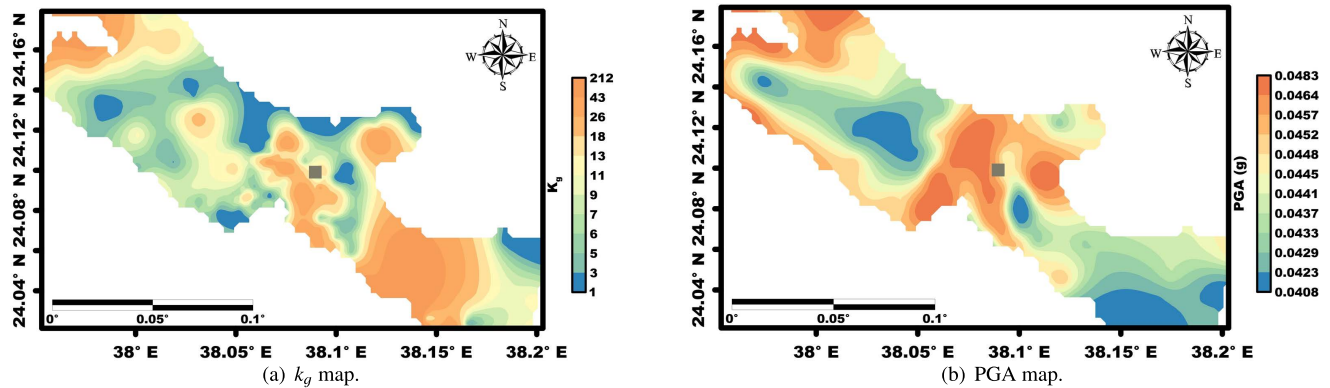
FIGURE 7. (a) Spatial distribution of the seismic vulnerability index k_g. (b) Contour map of the simulated peak ground acceleration in the mapped area utilizing the SMSIM stochastic ground motion simulation technique [106], [107].

lose strength, and behave as a viscous liquid, leading to very hazardous soil damage [110]. To identify areas susceptible to soil damage and/or liquefaction and to define the level of soil vulnerability to deformation, [111] used the seismic vulnerability index (k_g).

Damage to buildings due to seismic vibration depends very much on their structures and local geological conditions [16]. According to [111], damage from earthquake vibration can be minimized or controlled if the ground vulnerability index (calculated from HVSR microtremor data) is properly followed at the time of building construction. The seismic vulnerability index map prepared in this study (Figure 7(a)) reveals a wide range of k_g values (0.3–230). The majority of mapped areas are covered by the lowest k_g values and thus categorized as L or earthquake damage-free zones. The highest values of k_g are observed in the central and southern parts of the study area. These areas may suffer significantly from earthquakes emanating from nearby seismic source zones, especially from Zones 1 and 4 (Figure 3(b)).

Recently, a good correlation between k_g values and the distribution of earthquake damage was reported [112]. This index is therefore useful for the detection of weak zones (i.e. areas of unconsolidated sediment) during earthquakes. The k_g index map utilizes strains in local structures to identify potential hazard zones [110].

The estimated values of FF and SA parameters, obtained from HVSR analyses, enable the determination of k_g levels. Generally, areas that experience major damage from earthquakes attain k_g values of 20–100, whereas areas with less or no damage exhibit k_g values under five [110]. A contour map for the study area, as per the classification of k_g values, is given in Figure 7(a).

Many efforts have been exerted to study the strength of the shaking is commonly estimated by reference to intensity scales that describe the effects in qualitative terms [113]–[116]. Another important point of seismic hazard analysis is the assessment of ground motion attributes for a chosen site. PGA is frequently used as a hazard quantifier [2] and provides an overall quantitative approach to determining seismic hazard [117].

Unlike other studies that focus on the probabilistic seismic hazard assessment [118], [119], in this study, deterministic seismic hazard analysis (DSHA) was employed to calculate PGA values [120]. The DSHA approach uses known seismic sources sufficiently close to the site and available seismic source parameters and geological data to generate discrete, single-valued models of ground motion at the mapped site. Ground motions are estimated deterministically, given magnitude, source-to-site distance, and site conditions [121]. For DSHA and determination of PGA, seismicity parameters for each identified source zone were used to define the probable hazardous earthquake and its maximum credible magnitude (M_{max}) affecting the mapped area.

[122] noted that, for earthquakes with small to M magnitudes occurring over a large period, the frequency-magnitude distribution (FMD) can be used to estimate the seismicity parameter a (exhibits significant variations from region to region) and the b-value (related to the tectonic characteristics of the mapped region) to an acceptable degree of accuracy [123]. Furthermore, FMD can also be used to calculate the degree of completeness of the magnitudes (M_c) for each zone. In the present study, these parameters were determined through regression analysis of the FMD data [124] using the maximum likelihood method [125]. The maximum credible earthquake magnitude (M_{max}) was estimated using the Bayesian procedure [126], in which seismic parameters are treated as random variables and uncertainty of the b-value is taken into account.

Table 1 compares observed and predicted maximum credible earthquake magnitudes, with the b-values of the outlined source zones depicted in Figure 3(b).

Earthquake catalogs from various local and national/international sources were utilized to estimate various seismicity parameters (a, b, and M_c values). Figure 3(b) shows the spatial distribution of observed seismicity, which indicates that the study area is located at an L-seismic zone. However, H-intensity earthquakes in the surrounding area (such as the Al-Ays event) have created significant distress in the area. Large numbers of faults/lineaments systems can be detected within and around the study area. Nevertheless,

TABLE 1. Seismic hazard parameters for the four source zones.

Seismic Zone	Number of Events	a-value	b-value	M_c	Maximum observed magnitude	M_{max}
Z_1	4662	4.61	0.65 ± 0.08	2.6	5.7	6.5
Z_2	45	1.75	1.08 ± 0.06	2.49	4.2	5.2
Z_3	60	1.88	1.2 ± 0.07	2.79	3.9	4.7
Z_4	1553	3.58	0.552 ± 0.05	2.58	4.6	5.8

the most active systems are in the northeastern part which has produced relatively tangible earthquakes in the past ($3.5 < M_w < 5.7$). Based on the observed seismicity and the local tectonic framework, four source zones influencing the study area in different ways were delineated as shown in Figure 3(a). In the case of the first two zones (Z_1 and Z_2), the origin of peculiar seismicity is not yet properly known. Consequently, it is still unclear whether the seismicity in these zones is caused by magma intrusion through extensional faulting, tectonic processes, or temporal coupling/mechanical interaction between tectonic and magmatic processes [64]. Dense-clustering of earthquakes in the first and fourth seismic zones (See Figure 3(a)) is attributed to the accumulation of stresses as a result of intra-plate and rifting-related tectonic activity, respectively [54], [58], [59].

Table 1 indicates the obtained results of the FMD for each seismic zone that is computed by the maximum-likelihood method [125]. The L and b-values in Z_1 and Z_4 are well correlated with frequent occurrences of M to large magnitude earthquakes, whereas the higher b-values in Z_2 and Z_3 match well with the occurrence of L-magnitude earthquakes. M_{max} for these seismic zones were calculated using Kijko's Bayesian approach [126].

To identify controlling seismic sources for maximum potential ground motion in the four seismotectonic zones, the bedrock PGA value at Yanbu' city center was first empirically estimated using the regional attenuation relationship of [128]. For this purpose, the M_{max} value of each zone (Table 1) and its shortest distance from different sources was considered. The lowest PGA value of 0.02 g was ascertained for the third zone (Z_3), while the highest PGA value of 0.05 g was gauged to a maximum credible earthquake of $M_{max} = 6.7$ during the Al-Ays event.

In this case, the highest PGA value exceeded (by $> 23\%$) that of other seismic source zones. Consequently, the Al-Ays earthquake was selected as a controlling source for the assessment of the final DSHA and to obtain the various PGA values within the mapped region after incorporating source, attenuation, and site-specific characteristics.

Several researchers investigating strong ground motion synthesis using regular grid points have used the stochastic ground motion simulation technique [106]. This technique has also been successfully utilized for the estimation of PGA under various seismotectonic conditions [2], [129]–[133].

The method includes subdividing the fault plane into a certain number of sub-faults, each of which is assigned an ω^{-2} spectrum [134]–[136]. A slip distribution model,

derived from previous studies of the Al-Ays earthquake, was used to specifically account for the source effect. Contributions from all subfaults were then empirically attenuated to the observation sites, where they were summed to produce the synthetic acceleration time history. With this technique, the H-frequency part (in the range of 1–10 Hz) of the seismic signal is treated as a random function [137]. Model parameters used for the simulation analysis are listed in Table 2. The hypocentre distance from each grid point is taken to be the shortest distance from the lineament or fault. The cut-off frequency parameter ($f_{max} \approx 10$ Hz) is considered sufficient [137] to generate strong ground motion in the study area. The orientation of the fault model used in the present study was derived from the focal mechanism of the main shock (Figure 3(b)).

The dimensions of the fault were chosen based on the spatial distribution of the aftershocks that occurred during the first two hours after the mainshock and the source rupture process. To develop the PGA attribute layer and to avoid minor fluctuations, specific ranges of the predicted PGA values were zoned through contouring (Figure 7(b)). The PGA layer for the study area was classified into five broad classes, with the highest value of 0.05g observed in the central and northeastern parts and the lowest value of 0.03g recorded in the southeastern part of the study area.

Previous studies have indicated that H-frequency earthquake motions are taken as band-limited Gaussian noise with ω-squared mean spectrum [104], [131], [132], [134], [138]. For purposes of the present study, the ground motion of the 2009 Al-Ays earthquake was simulated using a widely applied stochastic method. The northern part of the study area (near the Al-Ays earthquake active zone) is characterized by higher PGA values compared to other parts (as evident from the PGA layer in Figure 7(b)). The southeastern part of Yanbu' city is, however, dominated by L to M PGA values.

V. DEVELOPED SEISMIC HAZARD, SUITABILITY ASSESSMENTS MAPS, AND RESULTS

A. ATTRIBUTES CLASSIFICATIONS

For the development of the final seismic hazard model, previously estimated thematic hazard parameters/layers were organized and further classified into sub-ranges using the equal interval division method. Spatial coverage of the utilized layers in the application of GIS was accomplished to enable the classification and grading of different spatial maps (Figures 4 - 7). The first and second layers, corresponding to SA and FF parameters, were incorporated to address

TABLE 2. Input parameters for the stochastic ground motion simulation method.

Parameter	Al-Ays earthquake mainshock
Fault orientation	Strike 337° , dip 43° ([127])
Fault dimension	29 × 13 km
Depth to the upper edge of the fault	2 km
Mainshock moment magnitude (Mmax)	6.5
Stress drop parameter	50 bars
Subfault dimensions	7.5 × 6.5 km
Number of subfaults	8
Number of subsources summed	6
Crustal shear-wave velocity	3.4 km/s
Crustal density	2.7 g/cm^3
Distance dependent duration term	Duration equal to rise time
Geometric spreading	1/hypocenter distance (R) for R< 100 km
Quality factor	Q = 353 f$^{0.88}$ ([127])
Windowing function	Saragoni-Hart
Cut-off frequency	10 Hz

generic hazard conditions affecting the distribution of urban and industrial buildings due to earthquake ground vibration. The third ST layer implicates the process by which seismic waves rebound, leading to SA. The fourth SS layer is defined on the principle of effective shear-wave velocity. The soil damage potential, measured in terms of k_g (the fifth layer), is recognized to be a determinant of urban seismic hazard, particularly for structures near natural water bodies. The final layer is the PGA, constituting the deterministic hazard based on the maximum expected magnitude (M_{max}) from nearby earthquake sources.

To derive the weight and rate for each layer, AHP analysis was applied to selected thematic layers. This involves clustering the decision problem into a hierarchy of more easily comprehended sub-cases that can be analyzed independently [24] and making judgments on the relative importance of pairs of elements and synthesizing results. Subsequently, the various layers affecting the seismic hazard model are evaluated systematically by comparing two simultaneously. In this respect, six parametric scales based on relative importance are assigned. The first scale gives equal importance to the two factors involved, while the sixth one indicates that one factor is more significant than the other. In addition, the corresponding reciprocals of these scales show that the first one is less important than the others [24]. In our case, the lowest importance was given to the SS layer, while the highest one was assigned to the FF layer. A higher ranking was assigned to the mapped area dominated by lower FF values, to facilitate hazard assessment.

Following the Saaty's comparison scale [92], [93], we have prioritized and classified the factors used in the implemented AHP approach, which has been implemented in the utilized Expert Choice software. Table 3 compares the assigned scales for achieving priority. Each class of these scales is ranked based on its expected seismic hazard potential. The assigned rankings for the Yanbu' Al-Bahr area are 1 2, 3, 4, and 5, corresponding to areas with VL, L, M, H, and VH seismic hazard potential, respectively. More particularly, these ranks have been adapted by the calculations done by a software package supporting the AHP, called Expert Choice. Corresponding ranks are then assigned to each thematic layer

according to its expected contribution to the overall seismic hazard potential and relative weights for each element of the hierarchy are computed. The initial integral ranking (R_i) of each thematic layer was normalized to ensure that no layer exerts an influence beyond its determined weight, as given by:

$$R_l = \frac{R_i - R_{min}}{R_{max} - R_{min}} \qquad (5)$$

where, R_{min}, and R_{max} denote the normalized, assigned minimum, and maximum ranks respectively. More concretely, R_l is a standard normalized equation from observed minimum and maximum values of the layer weight. The weights obtained for the six thematic layers were SS (0.2857), ST (0.2381), k_g (0.1905), PGA (0.1429), SA (0.0952), and FF (0.0476). Normalized ratings for these thematic layers are given in Table 4. A CR value of 0.0405 was obtained, indicating that the constructed matrix has an acceptable level of consistency [24] and a dynamic sensitivity analysis was applied to investigate the stability and consistency of the rankings under different weighting criteria. Figure 8 provides a tree diagram of all criteria and sub-criteria to determine the final implemented AHP weights.

Higher SA values (>3.97) can generally be observed along the coastal area with a relatively thick sedimentary cover. For constructing the AHP hierarchy, the SA layer was classified into five categories, i.e., VL (<0.78), L (0.78–2.38), M (2.38–3.97), H (3.97–5.57), and VH (>5.57) (Figure 9). Areas with H and VH SA values are the most vulnerable to earthquake-related hazards. On the other hand, and as indicated in Figure 9(b), the Yanbu' region exhibits varied FF values (from a minimum of 1.4 Hz to a maximum of 7.21 Hz). The majority of the mapped area reveals L FF values (1.4–2.57 Hz). However, some localized areas indicate M to VH FF values (most vulnerable places for future hazard events). The same five classes i.e. VL (<2.57), L (2.57–3.73), M (3.73–4.89), H (4.89–6.05), and VH (>6.05) were used to categorize the FF attribute layer.

V_S^{30} values for the study area stand between 180 m/s and 240 m/s, and SS values were classified into three categories: L (180–200 m/s), M (200–220 m/s), and H (>220 m/s)

TABLE 3. Pairwise comparison matrix of themes and their normalized weights.

Theme	SS	ST	k_g	PGA	SA	PF	Normalized weights
SS	1	1.2	1.5	2	3	6	0.2857
ST	0.84	1	1.25	1.67	2.5	5	0.2381
k_g	0.67		1	1.34	2	4	0.1905
PGA	0.5			1	1.5	3	0.1429
SA	0.34				1	2	0.0952
FF	0.17					1	0.0476
CR = 0.0405			$\lambda_{max} = 3.0731$				CI = 0.0365
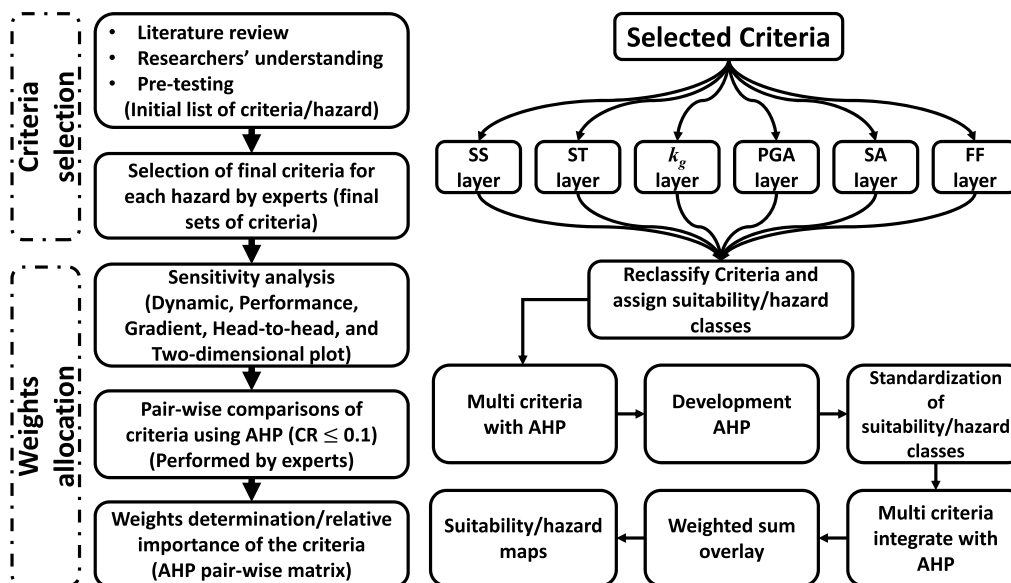
FIGURE 8. Criteria and sub-criteria to determine the final implemented AHP weights.
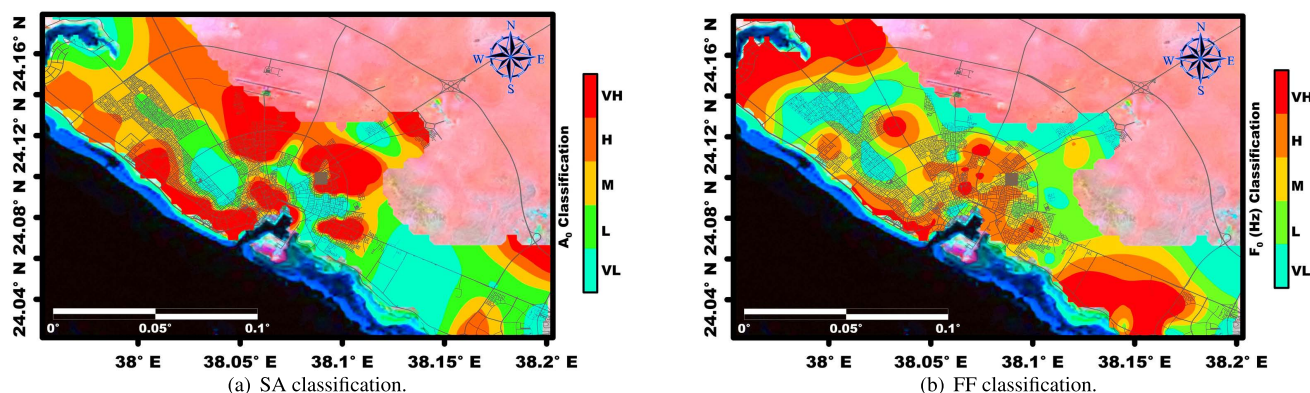

(a) SA classification.

(b) FF classification.

FIGURE 9. SA and FF thematic maps classifications.

(Figure 10(a)). The overburden thickness in the study was consequently found to vary between 2–15 m but is predominantly in a range of 3–6 m. The ST map prepared for the study area was thus classified into five categories: very thin (<3 m), thin (3–6 m), medium (6–9 m), thick (9–12 m), and very thick (>12 m) (Figure 10(b)). This shows that the most vulnerable areas to seismic hazards are those associated with thick to very thick sedimentary cover.

A contour map for the study area, as per the classification of Kg values, is given in Figure 11(a). This shows that, within the study area, Kg values are in the range of 0.3 and 230, and can be classified into four zones: L (<5), M (5–10), H (10–20), and VH (>20). The PGA layer for the study area was classified into five broad classes, with the highest value of 0.05g observed in the central and northeastern parts and the lowest value of 0.03g
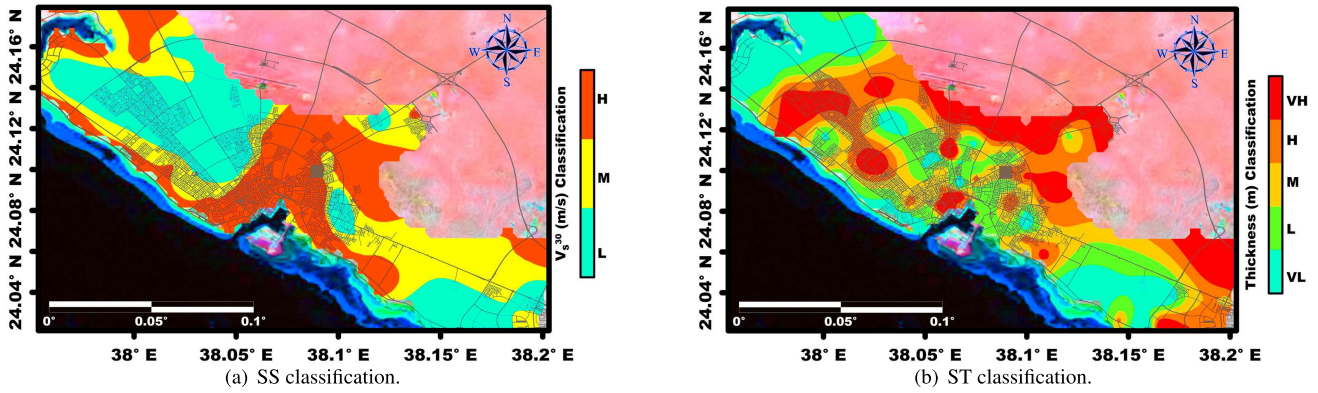
(a) SS classification.

(b) ST classification.

FIGURE 10. SS and ST thematic maps classifications.

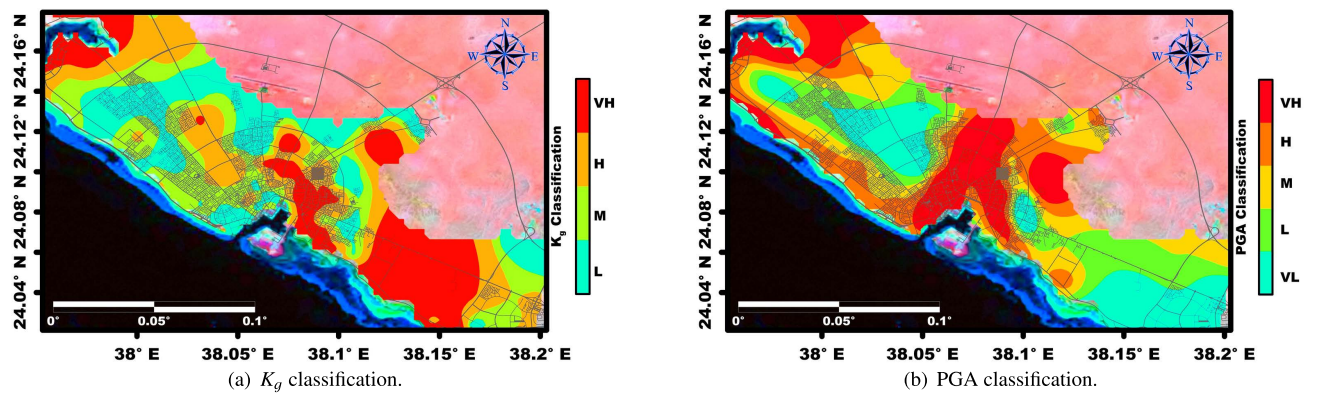(a) K_g classification.

(b) PGA classification.

FIGURE 11. K_g and PGA thematic maps classifications.

recorded in the southeastern part of the study area (Figure 11(b)).

It is worth mentioning that the AHP approach suffers from decision bias and rank reversal as well as many other decision-making approaches such as the Borda-Kendall (BK) method for aggregating ordinal preferences, the simple additive weighting (SAW) method, the technique for order preference by similarity to ideal solution (TOPSIS) method, and the cross-efficiency evaluation method in data envelopment analysis (DEA). However, in the current study, the used Expert Choice Software ensures that the rank reversal phenomena is managed and eliminated through the use of five types of sensitivity analysis built into Expert Choice: Dynamic (used to dynamically change the priorities of the objectives to determine how these changes affect the priorities of the available choices), Performance (shows how the alternatives were prioritized relative to other alternatives with respect to each objective as well as overall), Gradient (shows the alternatives' priorities concerning one objective at a time), Head-to-head (shows how two alternatives compared to one another against the objectives in a decision), and Two-dimensional plot (shows the alternatives' priorities for two objectives at a time).

B. HAZARDS AND APPROPRIATENESS

Several geological and seismological influential criteria were taken into consideration for the appraisal and categorization of Yanbu' in terms of its earthquake triggering attributes for urban developments. Due to the inclusion of many requirements/criteria, landuse appropriateness analysis has grown increasingly complex as a result of the principles of sustainable development.

Assigning relative weights to the many factors involved in determining the appropriateness of Yanbu' for urban development and land use was quite challenging. As a result, a strategy that allows for weight estimate using the AHP was utilized.

The GIS is a sophisticated tool for geographic and attributes data entry, storage, retrieval, modification, and analysis, as well as output. Land-use appropriateness analysis, on the other hand, necessitates the handling of both spatial and attribute data in several data layers. As a result, it's a good idea to utilize GIS to make use of its powerful geographical data processing capabilities. As a result, combining GIS and AHP with land suitability research is expected to yield positive results. The findings of using GIS and AHP to analyze land-use appropriateness are presented in this study.

TABLE 4. Normalized weights and ranks assigned to the respective themes and the features used for the thematic integration.

| Themes	Weight	Feature	Rank	Normalized Rank
SS	0.2857	180–200	1	0
		200–220	2	0.5
		220–240	3	1
	CR= 0.0018		λ_{max} = 1.9989	CI= 0.0011
ST	0.2381	<3	1	0
		3–6	2	0.25
		6–9	3	0.5
		9–12	4	0.75
		>12	5	1
	CR= 0.0844		λ_{max} = 4.2839	CI = 0.0946
k_g	0.1905	<5	1	0
		5–10	2	0.33
		10–20	3	0.66
		>20	4	1
	CR= 0.0959		λ_{max} = 6.6331	CI= 0.1266
PGA	0.1429		1	0
			2	0.25
			3	0.5
			4	0.75
			5	1
	CR= 0.0625		λ_{max} = 6.4134	CI= 0.0826
SA	0.0952	<0.78	1	0
		0.78–2.38	2	0.25
		2.38–3.97	3	0.5
		3.97–5.57	4	0.75
		>5.57	5	1
	CR= 0.0773		λ_{max} = 7.6652	CI= 0.0773
FF	0.0476	<0.891	1	0
		0.891–1.653	2	0.25
		1.653–2.641	3	0.5
		2.641–4.363	4	0.75
		>4.363	5	1
	CR= 0.0326		λ_{max} = 5.1621	CI= 0.0405
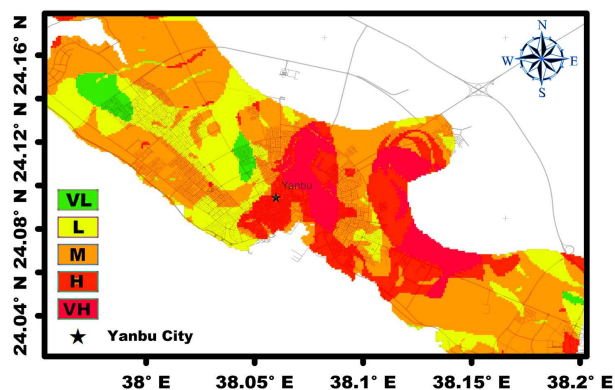
FIGURE 12. Seismic hazard index (SHI) map.

FIGURE 13. Site suitability in Yanbu' area.

Six criteria are utilized in the preparation of the final landuse suitability map. Each landuse thematic layer is organized in the form of one map layer in GIS. The overlay of these thematic map layers in GIS produces a composite map of urban development suitable and none suitable zones.

In this study, different scenarios were simulated for assigning weights to different layers. The expert judgment approach [139]–[141] was used initially to generate subsequent scenarios. For each criterion, the weight was increas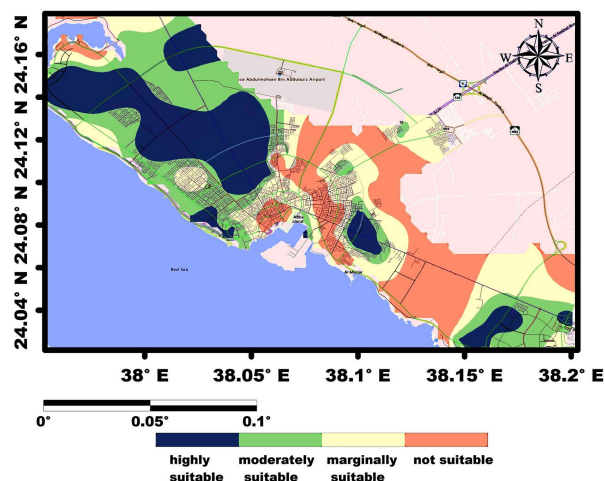ed by ≈5–9% after deducting this proportion equally from the weights of other criteria. All pairwise comparisons, eigenvectors, weights, and CRs were calculated using Expert Choice software [142].

In order to identify areas susceptible to potential seismic hazard risks, a powerful and flexible AHP technique was employed to construct a seismic hazard map for Yanbu' city, western Saudi Arabia. The AHP technique was used to generate an integrated seismic hazard map, with special emphasis

on the identification and characterization of major parameters that can affect the study area significantly. Based on AHP analysis, six hazard layers were indicated and an integrated seismic hazard map was produced using the GIS platform (Figure 12). It is worth noting that in the literature context, many efforts have been exerted to study the landslide effect on seismic hazard [143], [144]. However, the importance of this phenomenon, in the present study, these aspects are not considered remarkable factors because the digital elevation model of the studied area indicates a very low slope, which eliminates the chance of severe landslides. In the developed seismic hazard index map (See Figure 12), part of Yanbu' city is classified as an L-hazard zone, but with few pockets of H-hazard potential, especially in central parts and, to a lesser extent, southeastern parts (leading to the classification of the area as class D). The central H-hazard clusters are mainly attributed to thick sediment cover that is characterized by a relatively H shear-wave velocity (V_S^{30}). Other pockets of relatively H-hazard are located in the western part of the study area (along the Red Sea coast), possibly due to H susceptibility to liquefaction. Interestingly, the Class-C zones in the area exhibit an L level of hazard potential, which may be due to overburden thickness.

Finally, an integrated seismic hazard index (SHI) map for the study area was constructed after combining the six thematic layers along with their corresponding weights and ranks. Using the weighted linear combination method [36], all parameters were summed up after applying respective weights to each layer to yield an SHI map (Figure 12). Mathematically, the SHI summation is a standard equation from weight and rank of each layer (standard weighted sum), which can be expressed as equation (6), shown at the bottom of the page, where the subscripts *w* and *r* indicate the weight and ranking of the corresponding thematic layer. Based on the SHI values (ranging between 0.142 and 0.726), the SHI map was divided into five seismic hazard zones (VL, L, M, H, and VH). Areas with SHI values from 0.142 to 0.259 were qualitatively termed as VL-hazard zones, those with values of 0.259–0.376 as L-hazard zones, those with values of 0.376–0.492 as M-hazard zones, those with values of 0.492–0.609 as H-hazard zones, and those with values >0.609 as VH-hazard zones.

As evident from the map, H-hazard zones dominate the central part of the study area with notable sedimentary cover. The M and intermediate hazard regions are located in the terrain between the eastern and southern Yanbu' areas, while higher hilly areas exhibit an L to VL-hazard index. More specifically, Yanbu' city is located within an H-hazard zone and is surrounded by a VH seismic hazard zone. The land suitability map for Yanbu' is shown in Figure 13 has been created, based on the linear combination of each used

factor. The AHP method was applied to determine the relative importance of all selected factors. The total suitability score "Si" for each land unit (i.e., each raster cell in the map) was calculated from the linear combination of suitability score obtained for each factor and criteria involved. Each factor in the last layer was classified into four suitability classes and their suitability scores were presented in the standardized format ranging from least suitable to most suitable. Finally, the total suitability score from each factor was assembled to create a site suitability map depicted in Figure 13. The Building Seismic Safety Council (BSSC) [145], which deals with the complex technical, regulatory, social, and economic concerns involved in establishing and promulgating building earthquake risk-reduction procedures, was used to generate the final seismic hazard index map. This is why we divided our map into five categories in order to provide a decent overall estimate of the seismic risk in the region. For site-suitability categorization, on the other hand, we use the FAO Land suitability classifications to describe degrees of appropriateness [146], [147].

VI. CONCLUSION

Due to the western coast of Saudi Arabia being susceptible to natural disasters with vulnerability exacerbated by lack of preparation, it has become strictly desired to implement more investigations. Yanbu' Al-Bahr, a major Red Sea port, provides an excellent example. In this study, six hazard parameter layers have been considered. Besides, weight and rank values have been determined during AHP and assigned to each layer and its corresponding classes. We have integrated a seismic hazard map supported by GIS. Afterward, we have classified the study area into five hazard categories, namely, VL, L, M, H, and VH. It can be concluded from the final seismic hazard map that large parts of Yanbu' city and the wider surrounding area are prone to M to H levels of seismic hazard. The integrated seismic hazard index map constructed in this study thus provides a regional picture of seismic hazard zones in Yanbu' city and the surrounding areas, which can be used as a background map for planning any future construction taking into account the identified seismic risk zones. Furthermore, it is recommended that different stakeholders can use the seismic hazard map produced in the current study as a platform for future land-use planning and environmental hazard management. Finally, current research is an integrated approach to seismic hazard and site suitability development by identifying appropriate sites and constructing a methodology to assess sustainability by matching the characteristics of an area with those attributes most appropriate. This approach has been proven beneficial for supporting decision-making for planning urban facilities and resource utilization for sustainable development.

$$SHI = \frac{SS_w \times SS_r + ST_w \times ST_r + kg_w \times kg_r + PGA_w \times PGA_r + SA_w \times SA_r + FF_w \times FF_r}{\sum w} \qquad (6)$$

REFERENCES

[1] S. S. R. Moustafa, N. Alarifi, M. Naeem, and M. K. Jafri, "An integrated technique for delineating groundwater contaminated zones using geophysical and remote sensing techniques: A case study of Al-Quway'iyah, central Saudi Arabia," *Can. J. Earth Sci.*, vol. 51, no. 8, pp. 797–808, Aug. 2014.

[2] S. S. R. Moustafa and H. Takenaka, "Stochastic ground motion simulation of the 12 October 1992 Dahshour earthquake," *Acta Geophys.*, vol. 57, no. 3, pp. 636–656, Sep. 2009.

[3] A. Thornley, *Urban Planning Under Thatcherism: The Challenge Market*. Evanston, IL, USA: Routledge, 2018.

[4] S. L. Handy, M. G. Boarnet, R. Ewing, and R. E. Killingsworth, "How the built environment affects physical activity: Views from urban planning," *Amer. J. preventive Med.*, vol. 23, no. 2, pp. 64–73, 2002.

[5] J. M. Levy, *Contemporary Urban Planning*. Oxfordshire, U.K.: Taylor & Francis, 2016.

[6] F. C. Dai, C. F. Lee, and X. H. Zhang, "GIS-based geo-environmental evaluation for urban land-use planning: A case study," *Eng. Geol.*, vol. 61, no. 4, pp. 257–271, Sep. 2001.

[7] G. D. Bathrellos, D. P. Kalivas, and H. D. Skilodimou, "GIS-based landslide susceptibility mapping models applied to natural and urban planning in Trikala, central Greece," *Estudios Geológicos*, vol. 65, no. 1, pp. 49–65, Jun. 2009.

[8] T. Sitharam and P. Anbazhagan, "Seismic microzonation: Principles, practices and experiments," *EJGE Special Volume Bouquet*, vol. 8, p. 61, Jan. 2008.

[9] M. Salsabili, A. Saeidi, A. Rouleau, and M. Nastev, "Seismic microzonation of a region with complex surficial geology based on different site classification approaches," *Geoenvironmental Disasters*, vol. 8, no. 1, pp. 1–13, Dec. 2021.

[10] M. K. Akin, T. Topal, and S. L. Kramer, "A newly developed seismic microzonation model of Erbaa (Tokat, Turkey) located on seismically active eastern segment of the north Anatolian fault zone (NAFZ)," *Natural Hazards*, vol. 65, no. 3, pp. 1411–1442, Feb. 2013.

[11] K. L. Flores, C. R. Escudero, and A. Zamora-Camacho, "Multicriteria seismic hazard assessment in Puerto Vallarta metropolitan area, Mexico," *Natural Hazards*, vol. 105, no. 1, pp. 253–275, Jan. 2021.

[12] I. Pal, S. K. Nath, K. Shukla, D. K. Pal, A. Raj, K. K. S. Thingbaijam, and B. K. Bansal, "Earthquake hazard zonation of Sikkim Himalaya using a GIS platform," *Natural Hazards*, vol. 45, no. 3, pp. 333–377, Jun. 2008.

[13] O. R. Andriamihaja, F. Metz, J. G. Zaehringer, M. Fischer, and P. Messerli, "Identifying agents of change for sustainable land governance," *Land Use Policy*, vol. 100, Jan. 2021, Art. no. 104882.

[14] S. S. R. Moustafa, M. S. Abdalzaher, F. Khan, M. Metwaly, E. A. Elawadi, and N. S. Al-Arifi, "A quantitative site-specific classification approach based on affinity propagation clustering," *IEEE Access*, vol. 9, pp. 155297–155313, 2021.

[15] S. S. R. Moustafa, N. S. Al-Arifi, M. K. Jafri, M. Naeem, E. A. Alawadi, and M. A. Metwaly, "First level seismic microzonation map of Al-Madinah province, western Saudi Arabia using the geographic information system approach," *Environ. Earth Sci.*, vol. 75, no. 3, p. 251, Feb. 2016.

[16] A. Ansal, A. Kurtulus, and G. Tönük, "Seismic microzonation and earthquake damage scenarios for urban areas," *Soil Dyn. Earthq. Eng.*, vol. 30, no. 11, pp. 1319–1328, Nov. 2010.

[17] S. K. Nath and K. K. S. Thingbaijam, "Seismic hazard assessment—A holistic microzonation approach," *Natural Hazards Earth Syst. Sci.*, vol. 9, no. 4, pp. 1445–1459, Aug. 2009.

[18] A. G. Papadimitriou, A. A. Antoniou, G. D. Bouckovalas, and P. G. Marinos, "Methodology for automated GIS-aided seismic microzonation studies," *Comput. Geotechnics*, vol. 35, no. 4, pp. 505–523, Jul. 2008.

[19] T. Turk, U. Gümüşay, and O. Tatar, "Creating infrastructure for seismic microzonation by geographical information systems (GIS): A case study in the north Anatolian fault zone (NAFZ)," *Comput. Geosci.*, vol. 43, pp. 167–176, Jun. 2012.

[20] I. Linkov, F. K. Satterstrom, G. Kiker, C. Batchelor, T. Bridges, and E. Ferguson, "From comparative risk assessment to multi-criteria decision analysis and adaptive management: Recent developments and applications," *Environ. Int.*, vol. 32, no. 8, pp. 1072–1093, Dec. 2006.

[21] A. J. Niang, "Monitoring long-term shoreline changes along yanbu, kingdom of Saudi Arabia using remote sensing and GIS techniques," *J. Taibah Univ. Sci.*, vol. 14, no. 1, pp. 762–776, Jan. 2020.

[22] S. Almadani, A. Al-Amri, M. Fnais, K. Abdelrahman, E. Ibrahim, and E. Abdelmoneim, "Seismic hazard assessment for yanbu metropolitan area, western Saudi Arabia," *Arabian J. Geosci.*, vol. 8, no. 11, pp. 9945–9958, Nov. 2015.

[23] R. Jena, B. Pradhan, G. Beydoun, A. Al-Amri, and H. Sofyan, "Seismic hazard and risk assessment: A review of state-of-the-art traditional and GIS models," *Arabian J. Geosci.*, vol. 13, no. 2, pp. 1–21, Jan. 2020.

[24] T. L. Saaty, "Decision making with the analytic hierarchy process," *Int. J. Services Sci.*, vol. 1, no. 1, pp. 83–98, 2008.

[25] T. Erden and H. Karaman, "Analysis of earthquake parameters to generate hazard maps by integrating AHP and GIS for Küçükçekmece region," *Natural Hazards Earth Syst. Sci.*, vol. 12, no. 2, pp. 475–483, Feb. 2012.

[26] W. Ho and X. Ma, "The state-of-the-art integrations and applications of the analytic hierarchy process," *Eur. J. Oper. Res.*, vol. 267, no. 2, pp. 399–414, 2018.

[27] A. Abdelkarim, S. S. Al-Alola, H. M. Alogayell, S. A. Mohamed, I. I. Alkadi, and I. Y. Ismail, "Integration of GIS-based multicriteria decision analysis and analytic hierarchy process to assess flood hazard on the Al-Shamal train pathway in Al-Qurayyat Region, Kingdom of Saudi Arabia," *Water*, vol. 12, no. 6, p. 1702, Jun. 2020.

[28] T. Hilorme, K. Tkach, O. Dorenskyi, O. Katerna, and A. Durmanov, "Decision making model of introducing energy-saving technologies based on the analytic hierarchy process," *J. Manage. Inf. Decis. Sci.*, vol. 22, no. 4, pp. 489–494, 2019.

[29] G. D. Hasekioğulları and M. Ercanoglu, "A new approach to use AHP in landslide susceptibility mapping: A case study at yenice (Karabuk, NW Turkey)," *Natural Hazards*, vol. 63, no. 2, pp. 1157–1179, Sep. 2012.

[30] J.-F. Liu, J. Li, J. Liu, and R.-Y. Cao, "Integrated GIS/AHP-based flood risk assessment: A case study of Huaihe river basin in China," *J. Natural Disasters*, vol. 17, no. 6, pp. 110–114, 2008.

[31] M. S. Abdalzaher, O. Muta, K. Seddik, A. Abdel-Rahman, and H. Furukawa, "B-18-40 a simplified Stackelberg game approach for securing data trustworthiness in wireless sensor networks," in *Proc. IEICE Gen. Conf.*, 2016, p. 538.

[32] A. A. Malinowska and K. Dziarek, "Modelling of cave-in occurrence using AHP and GIS," *Natural Hazards Earth Syst. Sci.*, vol. 14, no. 8, pp. 1945–1951, Aug. 2014.

[33] K. Mishra and R. Sinha, "Flood risk assessment in the kosi megafan using multi-criteria decision analysis: A hydro-geomorphic approach," *Geomorphology*, vol. 350, Feb. 2020, Art. no. 106861.

[34] C. Çetinkaya, E. Özceylan, M. Erbaş, and M. Kabak, "GIS-based fuzzy MCDA approach for siting refugee camp: A case study for southeastern Turkey," *Int. J. Disaster Risk Reduction*, vol. 18, pp. 218–231, Sep. 2016.

[35] L. Albraheem and L. Alabdulkarim, "Geospatial analysis of solar energy in Riyadh using a GIS-AHP-based technique," *ISPRS Int. J. Geo-Inf.*, vol. 10, no. 5, p. 291, May 2021.

[36] O. Marinoni, "Implementation of the analytical hierarchy process with VBA in ArcGIS," *Comput. Geosci.*, vol. 30, no. 6, pp. 637–646, Jul. 2004.

[37] K. G. E. M. Khair, "Creating a Python toolbox to implement the analytical hierarchy process method in Arcgis," Ph.D. dissertation, Dept. Comput. Sci., Future Univ., Khartoum, Sudan, 2018.

[38] M. S. Abdalzaher and H. A. Elsayed, "Employing data communication networks for managing safer evacuation during earthquake disaster," *Simul. Model. Pract. Theory*, vol. 94, pp. 379–394, Jul. 2019.

[39] M. S. A. Alzaher, H. A. Elsayed, S. I. Kayed, and W. R. Anis, "Road traffic modeling using data communication networks," *Int. J. Comput. Appl.*, vol. 975, p. 8887, Jul. 2011.

[40] M. Elwekeil, M. S. Abdalzaher, and K. Seddik, "Prolonging smart grid network lifetime through optimising number of sensor nodes and packet length," *IET Commun.*, vol. 13, no. 16, pp. 2478–2484, Oct. 2019.

[41] M. S. Abdalzaher and O. Muta, "Employing game theory and TDMA protocol to enhance security and manage power consumption in WSNs-based cognitive radio," *IEEE Access*, vol. 7, pp. 132923–132936, 2019.

[42] M. S. Abdalzaher, K. Seddik, and O. Muta, "An effective Stackelberg game for high-assurance of data trustworthiness in WSNs," in *Proc. IEEE Symp. Comput. Commun. (ISCC)*, Jul. 2017, pp. 1257–1262.

[43] M. S. Abdalzaher, M. S. Soliman, S. M. El-Hady, A. Benslimane, and M. Elwekeil, "A deep learning model for earthquake parameters observation in IoT system-based earthquake early warning," *IEEE Internet Things J.*, vol. 9, no. 11, pp. 8412–8424, Jun. 2022.

[44] M. S. Abdalzaher and O. Muta, "A game-theoretic approach for enhancing security and data trustworthiness in IoT applications," *IEEE Internet Things J.*, vol. 7, no. 11, pp. 11250–11261, Nov. 2020.

[45] M. S. Abdalzaher, L. Samy, and O. Muta, "Non-zero-sum game-based trust model to enhance wireless sensor networks security for IoT applications," *IET Wireless Sensor Syst.*, vol. 9, no. 4, pp. 218–226, 2019.

[46] M. S. Abdalzaher, K. Seddik, M. Elsabrouty, O. Muta, H. Furukawa, and A. Abdel-Rahman, "Game theory meets wireless sensor networks security requirements and threats mitigation: A survey," *Sensors*, vol. 16, no. 7, p. 1003, 2016.

[47] M. S. Abdalzaher, K. Seddik, and O. Muta, "Using Stackelberg game to enhance cognitive radio sensor networks security," *IET Commun.*, vol. 11, no. 9, pp. 1503–1511, 2017.

[48] M. S. Abdalzaher, K. Seddik, O. Muta, and A. Abdelrahman, "Using Stackelberg game to enhance node protection in WSNs," in *Proc. 13th IEEE Annu. Consum. Commun. Netw. Conf. (CCNC)*, Jan. 2016, pp. 853–856.

[49] M. S. Abdalzaher, K. Seddik, and O. Muta, "Using repeated game for maximizing high priority data trustworthiness in wireless sensor networks," in *Proc. IEEE Symp. Comput. Commun. (ISCC)*, Jul. 2017, pp. 552–557.

[50] A. H. Alzalabani and D. Mzembe, "Employee empowerment in the royal commission at Yanbu," *China-USA Bus. Rev.*, vol. 11, no. 5, pp. 709–719, 2012.

[51] A. Behairy, A. Al-Kholy, M. Hashem, and K. El-Sayed, "Preliminary study on the geology and fisheries of the coastal area between Jeddah and Yanbu," *J. Fac. Mar. Sci.*, vol. 2, pp. 1–47, Jan. 1983.

[52] C. Pellaton, "Geologic map of the Yanbu'Al Bahr quadrangle, sheet 24c, Kingdom of Saudi Arabia," in *Saudi Arabian Deputy Ministry For Mineral Resources Geoscience Map GM A*, vol. 48. Kingdom of Saudi Arabia, Saudi Arabian Deputy Ministry for Mineral Resources, 1979.

[53] V. De Novellis, D. Reale, G. M. Adinolfi, E. Sansosti, and V. Convertito, "Geodetic model of the March 2021 thessaly seismic sequence inferred from seismological and InSAR data," *Remote Sens.*, vol. 13, no. 17, p. 3410, Aug. 2021.

[54] H. M. Merghelani, *Seismicity of the Yanbu region kingdom of Saudi Arabia*. Jeddah, Saudi Arabia: USGS Publications Warehouse, Ministry of Petroleum and Mineral Resources, 1981. [Online]. Available: https://pubs.er.usgs.gov/publication/70156973

[55] *Annual Report of the Strategic Planning and Investment Development*, Division Economic Planning Department, Royal Commission for Jubail and Yanbu, Riyadh, Saudi Arabia, 2013.

[56] A. A. Shehai, "Royal commission at Yanbu environmental regulations," *Proc. Eng.*, vol. 125, pp. 193–198, Jan. 2015.

[57] C. Pellaton, "Geologic map of the Al Madinah quadrangle, sheet 24d, kingdom of Saudi Arabia," in *Saudi Arabian Deputy Ministry For Mineral Resources Geoscience Map GM A*. Kingdom of Saudi Arabia, Saudi Arabian Deputy Ministry for Mineral Resources, 1981.

[58] Z. H. El-Isa and A. A. Shanti, "Seismicity and tectonics of the red sea and western Arabia," *Geophys. J. Int.*, vol. 97, no. 3, pp. 449–457, Jun. 1989.

[59] S. E.-H. Youssef, "Seismicity and seismotectonic setting of the red sea and adjacent areas," in *The Red Sea*. Cham, Switzerland: Springer, 2015, pp. 151–159.

[60] T. Aldaajani, K. Furlong, and R. Malservisi, "Arabian plate deformation: The role of inherited structures in the localization of strain in the red sea extensional system," in *AGU Fall Meeting Abstr.*, 2017, p. T51B.

[61] N. N. Ambraseys, C. P. Melville, and R. D. Adams, *The Seismicity of Egypt, Arabia and the Red Sea: A Historical Review*. Cambridge, U.K.: Cambridge Univ. Press, 2005.

[62] J. P. Poirier and M. A. Taher, "Historical seismicity in the near and middle east, north Africa, and Spain from Arabic documents (VIIth–XVIIIth century)," *Bull. Seismological Soc. Amer.*, vol. 70, no. 6, pp. 2185–2201, Dec. 1980.

[63] A. Al-Amri, B. Punsalan, A. Khalil, E. Uy, and S. S. Center, "Seismic hazard assessment of western Saudi Arabia and the red sea region," in *Proc. Bull. Interface Inst. Seismol. Earth Eng. (IISEE) Jpn. Spec. Ed.*, 2003, pp. 95–112.

[64] A. R. Blanchette, S. L. Klemperer, W. D. Mooney, and H. M. Zahran, "Mantle earthquakes in recently thinned neoproterozoic lithosphere: Harrat Lunayyir, Saudi Arabia," 2020, doi: 10.31223/X54S43.

[65] A. M. Al-Amri, K. Abdelrahman, R. Mellors, and D. Harris, "Seismic identification of geothermal prospecting in harrat rahat, northern Arabian shield," *Arabian J. Geosci.*, vol. 13, no. 8, pp. 1–7, Apr. 2020.

[66] M. F. Abdelwahed, N. N. El-Masry, A. Qaddah, M. R. Moufti, and F. Alqahtani, "Spatial distribution of the empirical peak ground motion in western Saudi Arabia and its implication on Al-Madinah city," *Arabian J. Geosci.*, vol. 13, no. 5, pp. 1–15, Mar. 2020.

[67] *International Seismological Centre on-Line Bulletin*, ISC, New Delhi, India, 2021.

[68] G. Ekström, M. Nettles, and A. M. Dziewoński, "The global CMT project 2004–2010: Centroid-moment tensors for 13,017 earthquakes," *Phys. Earth Planet. Interiors*, vols. 200–201, pp. 1–9, Jun. 2012.

[69] S. E.-H. Youssef, "Seismicity and seismotectonic setting of the red sea and adjacent areas," in *The Red Sea*. Cham, Switzerland: Springer, 2015, pp. 151–159.

[70] L. Sawade, W. Lei, S. Beller, F. Simons, and J. Tromp, "A database of global centroid moment tensors using 3d green's functions in model gladm25," in *Proc. AGU Fall Meeting Abstr.*, 2020, p. S047.

[71] S. Wimpenny and C. S. Watson, "GWFM: A global catalog of moderate-magnitude earthquakes studied using teleseismic body waves," *Seismological Res. Lett.*, vol. 92, no. 1, pp. 212–226, Jan. 2021.

[72] S. S. R. Moustafa, G.-E.-A. Mohamed, and M. Metwaly, "Production of a homogeneous seismic catalog based on machine learning for northeast Egypt," *Open Geosci.*, vol. 13, no. 1, pp. 1084–1104, Sep. 2021.

[73] S. S. R. Moustafa, M. S. Abdalzaher, M. H. Yassien, T. Wang, M. Elwekeil, and H. E. A. Hafiez, "Development of an optimized regression model to predict blast-driven ground vibrations," *IEEE Access*, vol. 9, pp. 31826–31841, 2021.

[74] M. S. Abdalzaher, S. S. R. Moustafa, M. Abd-Elnaby, and M. Elwekeil, "Comparative performance assessments of machine-learning methods for artificial seismic sources discrimination," *IEEE Access*, vol. 9, pp. 65524–65535, 2021.

[75] M. S. Abdalzaher, M. Elwekeil, T. Wang, and S. Zhang, "A deep autoencoder trust model for mitigating jamming attack in IoT assisted by cognitive radio," *IEEE Syst. J.*, early access, Aug. 10, 2021, doi: 10.1109/JSYST.2021.3099072.

[76] A. M. Al-Shanti, *Oolitic Iron Ore Deposits Wadi Fatima between Jeddah Mecca, Saudi Arabia*, no. 2. New Delhi, India: Ministry of Petroleum and Mineral Resources, 1966.

[77] J. Pallister, "Explanatory notes to the geologic map of the Al lith quadrangle, sheet 20d, kingdom of Saudi Arabia," in *Directorate General of Mineral Resources, Map GM-95C*. Kingdom of Saudi Arabia, Saudi Arabian Deputy Ministry for Mineral Resources, 1986.

[78] M. Al-Haddad, T. Al-Rrefeai, and A. Al-Amri, "Geotechnical investigation for earthquake resistance design in the kingdom (phase 1) western coast. Research project no," Funded King Abdulaziz City Sci. Technol., Riyadh, Saudi Arabia, Tech. Rep. AR-14-77, 2001.

[79] H. Al-Zahrani, M. Fnais, A. Al-Amri, and K. Abdel-Rahman, "Tectonic framework of Lunayyir area, northwest Saudi Arabia through aftershock sequence analysis of 19 May 2009 earthquake and aeromagnetic data," *Int. J. Phys. Sci.*, vol. 7, no. 44, pp. 5821–5833, 2012.

[80] K. S. Aldamegh, H. Hussein Moussa, S. N. Al-Arifi, S. S. R. Moustafa, and M. H. Moustafa, "Focal mechanism of Badr earthquake, Saudia Arabia of August 27, 2009," *Arabian J. Geosci.*, vol. 5, no. 4, pp. 599–606, Jul. 2012.

[81] Y. Nakamura, "A method for dynamic characteristics estimation of subsurface using microtremor on the ground surface," *Railway Tech. Res. Inst., Quart. Rep.*, vol. 30, no. 1, pp. 25–33, 1989.

[82] C. Lachetl and P.-Y. Bard, "Numerical and theoretical investigations on the possibilities and limitations of Nakamura's technique," *J. Phys. Earth*, vol. 42, no. 5, pp. 377–397, 1994.

[83] M. Mucciarelli, "Reliability and applicability of NJakamura's technique using microtremors: An experimental approach," *J. Earthq. Eng.*, vol. 2, no. 4, pp. 625–638, Oct. 1998.

[84] *Tromino'User's Manual*. Treviso, Italy: Micromed S.p.A., 2018.

[85] C. Acerra, H.-B. Havenith, and S. Zacharopoulos, "Guidelines for the implementation of the H/V spectral ratio technique on ambient vibrations measurements, processing and interpretation," Eur. Commission, Res. Gen. Directorate, Brussels, Belgium, Tech. Rep. EVG1-CT-2000-00026 SESAME, 2004. [Online]. Available: http://sesame.geopsy.org/Papers/HV_User_Guidelines.pdf

[86] P.-Y. Bard, "The H/V technique: Capabilities and limitations based on the results of the SESAME project," *Bull. Earthq. Eng.*, vol. 6, no. 1, pp. 1–2, Feb. 2008.

[87] M. S. Fnais, K. Abdelrahman, and A. M. Al-Amri, "Microtremor measurements in Yanbu city of western Saudi Arabia: A tool for seismic microzonation," *J. King Saud. Univ. Sci.*, vol. 22, no. 2, pp. 97–110, Apr. 2010.

[88] K. Alyousef, A. Al-Amri, M. Fnais, K. Abdelrahman, and O. Loni, "Site effect evaluation for yanbu city urban expansion zones, western Saudi arabia, using microtremor analysis," *Arabian J. Geosci.*, vol. 8, no. 3, pp. 1717–1729, Mar. 2015.

[89] M. Law and A. Colling, *Getting to Know ArcGIS Pro*, 2nd ed. Redlands, CA, USA: Esri press, 2016.

[90] E. ArcGIS, *10.7. 1: Geographical Information System*. West Redlands, CA, USA: ESRI, 2019.

[91] S. S. Moustafa, "Application of the analytic hierarchy process for evaluating geo-hazards in the Greater Cairo area, Egypt," *Electron. J. Geotech. Eng.*, vol. 20, no. 6, pp. 1921–1938, 2015.

[92] T. L. Saaty and L. T. Tran, "On the invalidity of fuzzifying numerical judgments in the analytic hierarchy process," *Math. Comput. Model.*, vol. 46, nos. 7–8, pp. 962–975, Oct. 2007.

[93] T. Saaty, *The Analytical Hierarchy Process*. New York, NY, USA: McGraw-Hill, 1980.

[94] J. A. Alonso and M. T. Lamata, "Consistency in the analytic hierarchy process: A new approach," *Int. J. Uncertainty, Fuzziness Knowl.-Based Syst.*, vol. 14, no. 4, pp. 445–459, Aug. 2006.

[95] M. L. Stein, *Interpolation Spatial Data: Some Theory for Kriging*. Cham, Switzerland: Springer, 2012.

[96] J.-P. Chilès and N. Desassis, "Fifty years of Kriging," in *Handbook of Mathematical Geosciences*. Cham, Switzerland: Springer, 2018, pp. 589–612.

[97] M. Power, R. Borcherdt, and J. Stewart, "Site amplification factors from empirical studies," Rep. Prepared Pacific Earthq. Eng. Res. Center, Univ. California, Berkeley, NGA Project Rep., Working Group 5, 2004, vol. 5.

[98] P. Anbazhagan, K. N. Srilakshmi, K. Bajaj, S. S. R. Moustafa, and N. S. N. Al-Arifi, "Determination of seismic site classification of seismic recording stations in the Himalayan region using HVSR method," *Soil Dyn. Earthq. Eng.*, vol. 116, pp. 304–316, Jan. 2019.

[99] T. L. Holzer, A. C. Padovani, M. J. Bennett, T. E. Noce, and J. C. Tinsley, "Mapping NEHRP VS30 site classes," *Earthq. Spectra*, vol. 21, no. 2, pp. 353–370, May 2005.

[100] S. Castellaro and F. Mulargia, "VS30 estimates using constrained H/V measurements," *Bull. Seismolog. Soc. Amer.*, vol. 99, no. 2A, pp. 761–773, Apr. 2009.

[101] *Grilla Software'User's Manual*. Treviso, Italy: Micromed S.p.A., 2018.

[102] B. Hassani and G. M. Atkinson, "Applicability of the site fundamental frequency as a VS30 proxy for central and eastern north America," *Bull. Seismolog. Soc. Amer.*, vol. 106, no. 2, pp. 653–664, Apr. 2016.

[103] M. Ibs-von Seht and J. Wohlenberg, "Microtremor measurements used to map thickness of soft sediments," *Bull. Seismolog. Soc. Amer.*, vol. 89, no. 1, pp. 250–259, Feb. 1999.

[104] S. Parolai, P. Bormann, and C. Milkereit, "Assessment of the natural frequency of the sedimentary cover in the cologne area (Germany) using noise measurements," *J. Earthq. Eng.*, vol. 5, no. 4, pp. 541–564, Oct. 2001.

[105] A. K. Mundepi and A. K. Mahajan, "Site response evolution and sediment mapping using horizontal to vertical spectral ratios (HVSR) of ground ambient noise in Jammu city, NW India," *J. Geolog. Soc. India*, vol. 75, no. 6, pp. 799–806, Jun. 2010.

[106] D. M. Boore, "Smsim-fortran programs for simulating ground motions from earthquakes: Version 2.3—A revision of OFR 96–80—A," U.S. Geological Surv. Open-File Rep., US Geological Surv. Open-File, Reston, VA, USA, Tech. Rep. 00–509, 2005, p. 55, vol. 15.

[107] D. M. Boore, "Smsim-fortran programs for simulating ground motions from earthquakes: Version 2.4—A revision of OFR 96–80—A," U.S. Geological Surv. Open-File Rep., U.S. Geolog. Surv. Open-File, Reston, VA, USA, Tech. Rep. 00–509, 2014.

[108] E. Seifert, "Originpro 9.1: Scientific data analysis and graphing software-software review," *J. Chem. Inf. Model.*, vol. 54, no. 5, p. 1552, 2014.

[109] J. G. Moberly, M. T. Bernards, and K. V. Waynant, "Key features and updates for origin 2018," *J. Cheminformatics*, vol. 10, no. 1, pp. 1–2, Dec. 2018.

[110] H.-C. Huang and Y.-S. Tseng, "Characteristics of soil liquefaction using H/V of microtremors in Yuan-Lin area, Taiwan," *Terr. Atmos. Ocean. Sci.*, vol. 13, no. 3, pp. 325–338, 2002.

[111] Y. Nakamura, "Real-time information systems for hazards mitigation," in *Proc. 11th World Conf. Earthq. Eng.*, 1996, pp. 23–28.

[112] S. Aswad, S. Amiruddin, D. Suriamiharja, and M. S. AP, "Mapping seismic vulnerability index on Hasanuddin area using spectral ratio for disaster prevention," White Paper, 2010, pp. 1–5. [Online]. Available: https://www.academia.edu/24930023

[113] K. Chousianitis, V. D. Gaudio, P. Pierri, and G.-A. Tselentis, "Regional ground-motion prediction equations for amplitude-, frequency response-, and duration-based parameters for Greece," *Earthq. Eng. Struct. Dyn.*, vol. 47, no. 11, pp. 2252–2274, Sep. 2018.

[114] K. W. Campbell and Y. Bozorgnia, "A ground motion prediction equation for the horizontal component of cumulative absolute velocity (CAV) based on the PEER-NGA strong motion database," *Earthq. Spectra*, vol. 26, no. 3, pp. 635–650, Aug. 2010.

[115] R. Foulser-Piggott and K. Goda, "Ground-motion prediction models for arias intensity and cumulative absolute velocity for Japanese earthquakes considering single-station sigma and within-event spatial correlation," *Bull. Seismolog. Soc. Amer.*, vol. 105, no. 4, pp. 1903–1918, Aug. 2015.

[116] E. M. Rathje, N. A. Abrahamson, and J. D. Bray, "Simplified frequency content estimates of earthquake ground motions," *J. Geotech. Geoenvironmental Eng.*, vol. 124, no. 2, pp. 150–159, Feb. 1998.

[117] J.-P. Wang, S.-C. Chang, Y.-M. Wu, and Y. Xu, "PGA distributions and seismic hazard evaluations in three cities in Taiwan," *Natural Hazards*, vol. 64, no. 2, pp. 1373–1390, Nov. 2012.

[118] M. Elhadidy, M. S. Abdalzaher, and H. Gaber, "Up-to-date PSHA along the Gulf of aqaba-dead sea transform fault," *Soil Dyn. Earthq. Eng.*, vol. 148, Sep. 2021, Art. no. 106835.

[119] M. S. Abdalzaher, M. El-Hadidy, H. Gaber, and A. Badawy, "Seismic hazard maps of Egypt based on spatially smoothed seismicity model and recent seismotectonic models," *J. Afr. Earth Sci.*, vol. 170, Oct. 2020, Art. no. 103894.

[120] K. Smith, *Environmental Hazards: Assessing Risk and Reducing Disaster*. Evanston, IL, USA: Routledge, 2013.

[121] A. Nekrasova, V. Kossobokov, A. Peresan, and A. Magrin, "The comparison of the NDSHA, PSHA seismic hazard maps and real seismicity for the Italian territory," *Natural Hazards*, vol. 70, no. 1, pp. 629–641, Jan. 2014.

[122] V. F. Pisarenko, D. Sornette, and M. V. Rodkin, "Distribution of maximum earthquake magnitudes in future time intervals: Application to the seismicity of Japan (1923–2007)," *Earth, Planets Space*, vol. 62, no. 7, pp. 567–578, Jul. 2010.

[123] O. Kulhanek, "Seminar on B-value," Dept. Geophys., Charles Univ., Prague, Czech Republic, Tech. Rep., 2005. [Online]. Available: http://karel.troja.mff.cuni.cz/magma/magma-051214.pdf

[124] B. Gutenberg and C. F. Richter, "Magnitude and energy of earthquakes," *Nature*, vol. 176, no. 4486, p. 795, 1955.

[125] S. Wiemer, "A software package to analyze seismicity: ZMAP," *Seismolog. Res. Lett.*, vol. 72, no. 3, pp. 373–382, May 2001.

[126] A. Kijko, "Estimation of the maximum earthquake magnitude, m max," *Pure Appl. Geophys.*, vol. 161, no. 8, pp. 1655–1681, Aug. 2004.

[127] A. K. Abdel-Fattah, A. M. Al-Amri, M. S. Fnais, and K. Abdelrahman, "Estimation of source parameters and attenuation using digital waveforms of Al-Ays 2009 earthquake, Saudi Arabia," *Arabian J. Geosci.*, vol. 7, no. 8, pp. 3325–3337, Aug. 2014.

[128] S. Akkar, M. A. Sandıkkaya, and J. J. Bommer, "Empirical ground-motion models for point- and extended-source crustal earthquake scenarios in Europe and the middle east," *Bull. Earthq. Eng.*, vol. 12, no. 1, pp. 359–387, Feb. 2014.

[129] M. Pischiutta, A. Akinci, E. Tinti, and A. Herrero, "Broad-band ground-motion simulation of 2016 Amatrice earthquake, central Italy," *Geophys. J. Int.*, vol. 224, no. 3, pp. 1753–1779, Dec. 2020.

[130] S. Karimzadeh, K. Kadas, A. Askan, and A. Yakut, "Comparison of real and simulated records using ground motion intensity measures," *Soil Dyn. Earthq. Eng.*, vol. 147, Aug. 2021, Art. no. 106796.

[131] A. Radu and M. Grigoriu, "A site-specific ground-motion simulation model: Application for Vrancea earthquakes," *Soil Dyn. Earthq. Eng.*, vol. 111, pp. 77–86, Aug. 2018.

[132] M. P. Moschetti and S. H. Hartzell, "Spectral inversion for seismic site response in central Oklahoma: Low-frequency resonances from the great unconformity," *Bull. Seismolog. Soc. Amer.*, vol. 111, no. 1, pp. 87–100, Feb. 2021.

[133] Y. M. A. Hashash, O. Ilhan, J. A. Harmon, G. A. Parker, J. P. Stewart, E. M. Rathje, K. W. Campbell, and W. J. Silva, "Nonlinear site amplification model for ergodic seismic hazard analysis in central and eastern north America," *Earthq. Spectra*, vol. 36, no. 1, pp. 69–86, Feb. 2020.

[134] J. N. Brune, "Seismic moment, seismicity, and rate of slip along major fault zones," *J. Geophys. Res.*, vol. 73, no. 2, pp. 777–784, Jan. 1968.

[135] H. Chen, C. Qu, D. Zhao, C. Ma, and X. Shan, "Rupture kinematics and coseismic slip model of the 2021 mw 7.3 maduo (China) earthquake: Implications for the seismic hazard of the Kunlun fault," *Remote Sens.*, vol. 13, no. 16, p. 3327, Aug. 2021.

[136] S. Markušić, D. Stanko, D. Penava, I. Ivančić, O. B. Oršulić, T. Korbar, and V. Sarhosis, "Destructive M6.2 petrinja earthquake (Croatia) in 2020—Preliminary multidisciplinary research," *Remote Sens.*, vol. 13, no. 6, p. 1095, Mar. 2021.

[137] D. M. Boore, "Simulation of ground motion using the stochastic method," *Pure Appl. Geophys.*, vol. 160, no. 3, pp. 635–676, Mar. 2003.

[138] E. Ghamry, E. K. Mohamed, M. S. Abdalzaher, M. Elwekeil, D. Marchetti, A. D. Santis, M. Hegy, A. Yoshikawa, and A. Fathy, "Integrating pre-earthquake signatures from different precursor tools," *IEEE Access*, vol. 9, pp. 33268–33283, 2021.

[139] H. Otway and D. von Winterfeldt, "Expert judgment in risk analysis and management: Process, context, and pitfalls," *Risk Anal.*, vol. 12, no. 1, pp. 83–93, Mar. 1992.

[140] K. J. Mach, M. D. Mastrandrea, P. T. Freeman, and C. B. Field, "Unleashing expert judgment in assessment," *Global Environ. Change*, vol. 44, pp. 1–14, May 2017.

[141] N. C. Brownstein, T. A. Louis, A. O'Hagan, and J. Pendergast, "The role of expert judgment in statistical inference and evidence-based decision-making," *Amer. Statistician*, vol. 73, no. 1, pp. 56–68, Mar. 2019.

[142] E. Choice, *Decision Support Software*. Pittsburgh, PA, USA: Expert Choice Inc., 2019.

[143] X. Fan, G. Scaringi, O. Korup, A. J. West, C. J. Westen, H. Tanyas, N. Hovius, T. C. Hales, R. W. Jibson, K. E. Allstadt, L. Zhang, S. G. Evans, C. Xu, G. Li, X. Pei, Q. Xu, and R. Huang, "Earthquake-induced chains of geologic hazards: Patterns, mechanisms, and impacts," *Rev. Geophys.*, vol. 57, no. 2, pp. 421–503, Jun. 2019.

[144] M. Karpouza, K. Chousianitis, G. D. Bathrellos, H. D. Skilodimou, G. Kaviris, and A. Antonarakou, "Hazard zonation mapping of earthquake-induced secondary effects using spatial multi-criteria analysis," *Natural Hazards*, vol. 109, no. 1, pp. 637–669, Oct. 2021.

[145] *National Earthquake Hazards Reduction Program Recommended Provisions for Seismic Regulations for New Buildings and Other Structures (FEMA-450)—Part 1: Provisions*, Bharat Sevak Samaj Council, Federal Emergency Manage. Agency, Washington, DC, USA, 2003, vol. 303.

[146] J. S. Latham, C. He, L. Alinovi, A. DiGregorio, and Z. Kalensky, "FAO methodologies for land cover classification and mapping," in *Linking People, Place, Policy*. Cham, Switzerland: Springer, 2002, pp. 283–316.

[147] W. Verheye, A. Koohafkan, and F. Nachtergaele, "The FAO guidelines for land evaluation," *Encyclopedia land Use, Land Cover Soil Sci., Land Eval.*, vol. 2, pp. 78–100, Sep. 2009.

SAYED S. R. MOUSTAFA received the B.Sc. degree in geophysics from Cairo University, Egypt, in 1990, the M.Sc. and Ph.D. degrees in geophysics from Ain Shams University, Cairo, Egypt, in 1997 and 2002, respectively, and the Diploma degree in seismology and earthquake engineering from the International Institute of Seismology and Earthquake Engineering (IISEE), Japan, in 2001.

Since December 1994, he has been with the Egyptian National Seismic Network Laboratory (ENSN), Department of Seismology, National Research Institute of Astronomy and Geophysics, Cairo, where he was an Assistant Professor; became an Associate Professor, in 1998; and a Professor, in 2002. From 2009 to 2019, he was a Professor with the Geology and Geophysics Department, College of Science, King Saud University, Saudi Arabia. Currently, he is the Head of the Egyptian National Seismic Network Laboratory, Seismology Department, National Research Institute of Astronomy and Geophysics. His current research interests include earthquake rupture mechanics, numerical methods for wave propagation, spectral element method for ground motion simulation, site response and seismic hazard, characterization of sedimentary basins, and simulation of their seismic response. He is a member of the American Geophysical Union (AGU), the Society of Exploration Geophysicists (SEG), and the Egyptian Geophysical Society (EGS).

MOHAMED S. ABDALZAHER (Senior Member, IEEE) received the B.Sc. degree (Hons.) in electronics and communications engineering, in 2008, the M.Sc. degrees in electronics and communications engineering from Ain Shams University, Cairo, Egypt, in 2012, and the Ph.D. degree from the Electronics and Communications Engineering Department, Egypt-Japan University of Science and Technology, Madinet Borg Al Arab, Egypt, in 2016.

He is an Associate Professor with the Seismology Department, National Research Institute of Astronomy and Geophysics, Cairo. He was a special research student with Kyushu University, Fukuoka, Japan, from 2015 to 2016. In April 2019 to October 2019, he was with the Center for Japan-Egypt Cooperation in Science and Technology, Kyushu University, where he was a Postdoctoral Researcher. His research interests include earthquake engineering, data communication networks, wireless communications, WSNs security, the IoT, and deep learning.

Dr. Abdalzaher is a TPC Member of the Vehicular Technology Conference and International Japan-Africa Conference on Electronics, Communications and Computers and a Reviewer of the IEEE Internet of Things Journal, IEEE Systems Journal, IEEE Access, *Transactions on Emerging Telecommunications Technologies*, *Applied Soft Computing*, *Journal of Ambient Intelligence and Humanized Computing*, and IET journals.

MUHAMMAD NAEEM was a Research and Teaching Assistant with the Department of Geology and Geophysics, King Saud University, Riyadh, Saudi Arabia, from 2012 to 2015. He has been a Geophysicist with the Exploration Department, Mari Petroleum Company Ltd., Islamabad, Pakistan, since 2015.

MOSTAFA M. FOUDA (Senior Member, IEEE) received the Ph.D. degree in information sciences from Tohoku University, Japan, in 2011. He is currently an Assistant Professor with the Department of Electrical and Computer Engineering, Idaho State University, ID, USA. He also holds the position of Associate Professor with Benha University, Egypt. He has served as an Assistant Professor with Tohoku University, Japan. He was a Postdoctoral Research Associate with Tennessee Technological University, TN, USA. He has published more than 60 papers in prestigious peer-reviewed journals and conferences. He has been engaged in research on cybersecurity, communication networks, signal processing, wireless mobile communications, smart healthcare, smart grids, AI, blockchain, and the IoT. He was a recipient of the prestigious 1st place award during his graduation from the Faculty of Engineering at Shoubra, Benha University, in 2002. He has served as the Symposium/Track Chair for IEEE VTC 2021-Fall Conference. He has also served as the Workshop Chair, the Session Chair, and a Technical Program Committee (TPC) Member in leading international conferences like IEEE GLOBECOM, ICC, PIMRC, ICCVE, IWCMC, and 5G World Forum. He also served as a Guest Editor for some special issues of several top-ranked journals such as IEEE Wireless Communications (WCM) and *IEEE Internet of Things Magazine* (IoTM). He also serves as a Referee for some renowned IEEE journals and magazines such as IEEE Communications Surveys and Tutorials, *IEEE Wireless Communications Magazine*, IEEE Wireless Communications, IEEE Transactions on Parallel and Distributed Systems, IEEE Transactions on Smart Grid, IEEE Access, IEEE Transactions on Network and Service Management, IEEE Transactions on Emerging Topics in Computing, and *IEEE Network*. He is an Editor of IEEE Transactions on Vehicular Technology (TVT) and an Associate Editor of IEEE Access.

● ● ●